CHALMERS
UNIVERSITY OF TECHNOLOGY

Sensitivity of P- and L-band SAR Tomography to Above-Ground Biomass in a Hilly Temperate Forest

Sensitivity of P- and L-band SAR Tomography to Above-Ground Biomass in a Hilly Temperate Forest

Patrik J. Bennet, Lars M. H. Ulander, Mauro Mariotti D'Alessandro and Stefano Tebaldini

***Abstract*—Tomographic Synthetic Aperture Radar (TomoSAR) is a promising technique for estimation of forest Above-Ground Biomass (AGB), but knowledge gaps still remain concerning the effects of forest type and ground topography. The paper presents new results at P- and L-band based on data acquired during the TomoSense campaign. The study area is a temperate forest, predominantly beech and spruce, with ground slopes ranging up to 40°. Analysis of vertical reflectivity profiles show distinct differences for spruce and beech. Three AGB retrieval methods are analysed, i.e. total vertical backscatter I_{tot}, canopy backscatter from a height layer I_c, and the ratio $I_{cr} = I_c/I_{tot}$. All three methods show sensitivity to AGB for spruce, whereas for beech this is only true for the two latter methods. For P-band, a significant ground slope effect is observed, while less so for L-band. The highest R^2 is obtained for spruce with HV-polarisation, I_c and ground slopes less than 10°, i.e. R^2 = 0.86 and RMSE = 15.6% for P-band and R^2 = 0.75 and RMSE = 12.5% for L-band. Corresponding results by including all forest types are R^2 = 0.77 and RMSE = 11.4% for P-band and R^2 = 0.54 and RMSE = 12.0% for L-band. Moreover, performance of using I_{cr} is similar to that of I_c. The ratio I_{cr} can be determined without absolute radiometric calibration which relaxes system requirements. This paper reinforces the potential of TomoSAR for forest AGB estimation and draws attention to important effects of tree species and ground slope.**

***Index Terms*—P-band, L-band, TomoSAR, temperate forest, ground slope, AGB retrieval.**

I. Introduction

FOREST biomass monitoring plays a key role in understanding the Earth's carbon cycle and thereby the global climate system [1]–[3]. However, accurate large coverage estimation of biomass is challenging. The uncertainties of current remote sensing data products are relatively large, which leaves this part of the climate system poorly quantified and obscures the analysis of carbon flux and stock [4]. Current forest biomass estimation from satellite is done through optical, thermal or near infrared spectrometer, lidar, radiometer or Synthetic Aperture Radar (SAR) sensors. A radar operating at longer wavelengths, i.e. a few decimeters and longer, has the capability to penetrate through clouds and into forest canopies while being sensitive to tree stems and branches, containing a majority of the Above-Ground Biomass (AGB). Shorter wavelengths are sensitive to smaller structures, which means that radars operating at different frequency bands provide complimentary information of the forest structure (e.g. X-band observes mainly the canopy, while P-band mainly the trunks) [5], [6]. One of the most promising techniques for improved biomass monitoring is Tomographic SAR (TomoSAR) observing in the P- and L-band frequency range, with wavelengths about 0.2 to 1 m [4]. Compared to regular 2D SAR imaging, tomographic techniques can resolve the vertical distribution of reflectivity in the forest, conveying information of the vertical structure that can be utilized to improve AGB estimates. In the near future the BIOMASS mission, ESA's 7:th Earth Explorer satellite, will be launched, carrying a P-band SAR for remote sensing of the Earth's forests [3], [7]. This is the very first spaceborne mission with TomoSAR capabilities, planned for launch in 2025. While the BIOMASS satellite is underway, there is still a lot to be learnt about forest AGB estimation through TomoSAR observations.

Manuscript received October 30, 2023; revised March 14, 2024.

P. J. Bennet and L. M. H. Ulander are with the Department of Space, Earth and Environment, Chalmers University of Technology, 412 96 Gothenburg, Sweden (e-mail: patrik.bennet@chalmers.se).

M. Mariotti D'Alessandro and S. Tebaldini are with Politecnico di Milano, 20133 Milan, Italy.

We acknowledge support from ESA under ESA/ESTEC contract TOMOSENSE: Technical Assistance for Airborne Measurements during the Tomographic Sensing Experiment, ESA, 4000127285/19/NL/FF/gp.

A. Review of TomoSAR forest AGB sensitivity

The analysis presented in this paper should be seen in the context of previous forest TomoSAR studies, which are here given a brief review. AGB sensitivity and retrieval have been analysed mainly over tropical or boreal forest sites [8]–[15], but there has also been one study over a temperate forest site [16]. TomoSAR forest AGB retrieval was evaluated in e.g. [8]–[10] using a power law relating backscatter and AGB, which has been used extensively for SAR [17].

The BioSAR-1 (2007) and -2 (2008) campaigns provided P- and L-band TomoSAR observations over a hemi-boreal and a boreal forest site, Remningstorp and Krycklan respectively, located in Sweden. In Remningstorp, the topography was fairly flat (no significant ground slope) and the mean AGB was reaching up to about 260 t/ha with a mean of 120 t/ha. P-band TomoSAR was done by combining 9 SAR flight tracks (baselines), resulting in a vertical resolution of 10 to 52 m [8]. In Krycklan, many ground slopes were up to 15° and 6 baselines were flown, yielding a vertical resolution of 21 to 104 m at P-band and 5 to 20 m at L-band [8], [18]. AGB ranged up to 260 t/ha with a mean about 90 t/ha. AGB retrieval was evaluated for P-band with training residuals resulting in an R^2 of 0.50-0.70 and an RMSE of 27-33 t/ha (30-36 %) for HV [8]. At L-band, an R^2 of 0.67 and an RMSE of 23 t/ha (25 %) was obtained for HH [9]. The intensity integral between 10 and 30 m height was related to AGB through a power law model in both these studies [8], [9].

The TropiSAR (2009) and AfriSAR (2015-2016) campaigns resulted in P- and L-band TomoSAR observations over tropical forest sites [10]–[15], [19]. TropiSAR covered two main sites,

Paracou and Nouragues, in French Guiana. In Paracou, some ground slopes up to around 20° were present and the AGB ranged from about 250 to 400 t/ha, while forest height ranged from 20 to over 40 m [10]. The P-band vertical resolution was about 20 m, resulting from 6 flown baselines. The study concluded that the highest sensitivity of P-band TomoSAR intensity to AGB was found in the 30 m height layer, where $R^2 = r_p^2$ was 0.71 (where the Pearson correlation coefficient r_p was 0.84) and the RMSE 35 t/ha (9.4 %) at HV [10]. A power law model was used to relate TomoSAR intensity and AGB. The Nouragues site was considerably more topographic than the Paracou site, while the ground slopes were still at most 20° [11]. In a cross-validation study between the Paracou and Nouragues sites, the overall P-band TomoSAR AGB sensitivity was still highest in the 30 m height layer and it showed an R^2 of 0.56 (r_p was 0.75) and RMSE of 55 t/ha (15.3 %) at HV [11]. A further study of the Paracou P-band data set reinforced the earlier results on high AGB sensitivity in the 30 m height layer at HV, additionally concluding that AGB estimation using TomoSAR intensity outperformed AGB estimation using lidar forest height information [12]. Many different models were evaluated, at best showing an R^2 of 0.92 and RMSE of 14 t/ha (4.1 %).

AfriSAR resulted in joint ESA/NASA P- and L-band TomoSAR imaged forest sites in Lopé National Park, Mabounié and Rabi, located in Gabon [13]–[15], [19]. P-band TomoSAR was done by ESA using 8-10 baseline flight tracks, providing a vertical resolution between 10 to 15 m [19]. Correspondingly, L-band TomoSAR was done by NASA over Lopé and Rabi using 8 baselines, resulting in a vertical resolution of about 8 m [15]. In Lopé, some ground slopes were as steep as 30° [13] and the biomass ranged from 60 to 600 t/ha [19]. An AGB sensitivity analysis of the combined AfriSAR Lopé and TropiSAR Paracou P-band TomoSAR data sets yielded an R^2 of 0.94 (r_p = 0.97) in the 30 m height layer at HV [14]. A study of P/L-band TomoSAR forest AGB retrieval over the Lopé site indicated an R^2 of 0.88/0.81 and RMSE of 48/62 t/ha (13/17 %), using a power law model and the 40 to 50 m height intensity integral [20]. Another study regard the use of P- and L-band TomoSAR to estimate forest structure parameters [13], which could in turn be used to estimate AGB through empirical relations (similarly as was done in [16]).

DLR conducted TomoSAR acquisitions at P-, L- and X-band over a temperate forest site in Traunstein, Germany, consisting of dominant spruce forest, with ground slopes below about 10° [16], [21]. TomoSAR AGB retrieval was only evaluated at L-band and the vertical minimum Rayleigh resolution was about 15 m, a result of combining 5 baselines, and forest stand heights ranged from 10 to 40 m [16]. Empirical relations were used to estimate forest AGB, reaching up to about 350 t/ha with a mean of 200 t/ha. This was done both before and after rain. Under dry conditions, an R^2 of 0.77/0.72 and RMSE of 38/43 t/ha was obtained using HH/HV respectively. After rain, an R^2 of 0.80/0.77 and an RMSE of 36/39 t/ha was obtained for L-band at HH/HV [16]. This shows that dielectric changes due to precipitation affects the TomoSAR AGB sensitivity characteristics. Although, the Capon spectral estimator was used to gain superresolution in the TomoSAR profiles, which performance is mentioned to be better for moist than for dry conditions [16].

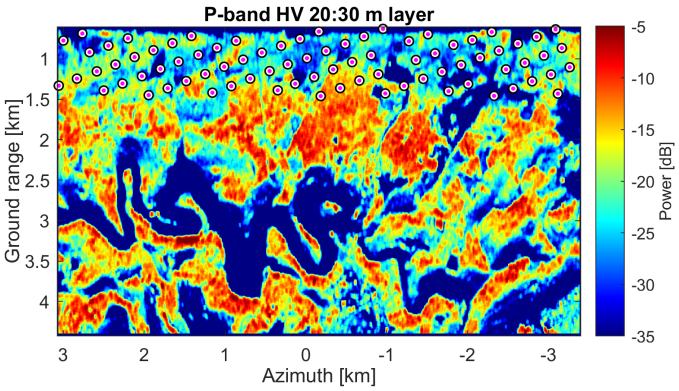

Fig. 1. P-band TomoSAR HV 20 to 30 m height layer intensity. The locations of the 80 in-situ plots are marked by the white circles with magenta center points. The intensity is averaged using a square window with 30 m sides.

B. The novelty of this study

The TomoSense campaign's TomoSAR forest observations are unique: the vertical resolution of 5 to 15 m at P-band and the large coverage of sloping terrain enable new and more detailed analyses. In this paper, we analyse the forest AGB sensitivity of TomoSAR, distinguishing between temperate, beech, and spruce forest types. Notably, we observe differences in AGB dependence between spruce and beech forests' vertical reflectivity profiles at the landscape level, as detailed in Section IV. Section V evaluates TomoSAR AGB retrieval using a power law model, highlighting the promising performance of a normalized intensity method. Section VI addresses the influence of ground slope on AGB retrieval performance, particularly evident at P-band.

II. Data and processing

The TomoSense ESA campaign has provided the scientific community with a rich dataset for research on P- and L-band TomoSAR remote sensing of temperate forests. In addition to this, the data collected also includes C-band SAR acquisitions, in-situ forest inventory, Airborne Lidar Scanning (ALS) canopy height and AGB estimation maps, Terrain Lidar Scanning (TLS) plots and areas covered by Unmanned Aerial Vehicle Lidar (UAV-L) [22]. This provides a solid basis for analysis of forest remote sensing techniques. The test site is located within the Kermeter area in the Eifel National Park in North Rhine-Westphalia, Germany. Many ground slopes are larger than 20°, reaching even 40° in some parts of the forest. A forest biotype inventory map covering the test site enabled a segmentation of forest types. The two dominant species in the area of the radar acquisitions were beech (European beech, *Fagus sylvatica*) and spruce (Norway spruce, *Picea abies*).

SAR flights at P-, L- and C-band were carried out by MetaSensing, ALS was done by CzechGlobe, forest inventory and in-situ data was provided by Landesbetrieb Wald und Holz (WuH) and TLS and UAV-L was done by University College London and Wageningen University & Research. The

processing of the SAR flight data to complex TomoSAR cubes was done by Politecnico di Milano. 5 m large trihedral corner reflectors for SAR calibration was provided by the Swedish Defence Research Agency (FOI). Particular focus will be put on describing how the P- and L-band TomoSAR data sets and the ALS AGB estimation map were obtained, since they have been used directly to produce the herein presented results.

A. TomoSAR processing

SAR images were acquired across two headings, i.e. along North-West (NW) and South-Eeast (SE) directed flight tracks, observing two in near-range slightly overlapping areas. Data sets were produced independently for each heading. The P-band TomoSAR products were processed using Single Look Complex (SLC) images from 28 SAR flight passes. 19 passes occurred on the 22nd of July 2020 and 9 additional ones on the 23rd. For each acquisition heading, the passes covered a height variation of 40 m. A center frequency of 435 MHz was used, with a bandwidth of 30 MHz [22]. The resolution is 5 m in slant range, 1 m in azimuth and about 5 to 15 m vertically over the area used for the analysis in this study. Correspondingly, the L-band mono-static (MS) and bi-static (BS) TomoSAR products are constructed from 30 flight passes each, where SAR flights occurred on the 14th, 15th and 16th of September 2020. The passes were swept over a height variation of 80 m, while the airplane with the BS receiver was kept at a constant altitude. The center frequency was 1.375 GHz, with a 50 MHz bandwidth [22]. The resolution is 3 m in slant range, 0.55 m in azimuth and vertically less than 5 m for MS data and less than 5 to about 7 m for BS data.

The basic principle of TomoSAR processing is to combine multiple approximately parallel SAR flight tracks. This creates a 2D aperture, which enables a 3D localization of the radar echoes. The P-, L- MS and L-band BS data were processed by direct back-projection using all available SLC images within each data-stack as described in [23]. That is, expressing the pixel s_n in each (calibrated) SLC image as

$$s_n = \int r(z) \exp\left(j \frac{4\pi}{\lambda} \frac{b_n}{R_n \sin(\theta)}\right) dz, \tag{1}$$

where $r(z)$ is the vertical distribution of the complex reflectivity within the SAR resolution cell, b_n the interferometric baseline, R_n the range distance from the scattering element to a radar sensor in the nth trajectory and θ the off-nadir angle. As can be noted, Eq. 1 is expressed on the form of a Fourier transform. The complex reflectivity $r(z)$ can then be retrieved by taking the inverse Fourier transform with respect to the N interferometric baselines (assumed equi-distant) as

$$\hat{r}(z) = \sum_{n}^{N} s_n \exp\left(-j \frac{4\pi}{\lambda} \frac{b_n}{R_n \sin(\theta)} z\right). \tag{2}$$

Eq. 2 is a simplified approach that provides an immediate understanding of the basics of tomographic processing, where more specific details have been discussed in [24], [25]. The resulting power of the voxels in a tomographic layer over 20 to 30 m height at P-band is shown in Fig. 1, averaged using a square window with 30 m sides.

Focused SLC images were provided in ground coordinates, geolocated and co-registered with each other. Range delay due to internal instrumentation were estimated using the corner reflectors, optimizing the range direction co-registration. Radiometric calibration was applied using information of the corner reflectors, antenna radiation patterns and an estimation of channel imbalances. A few further calibration steps were deemed necessary, to mitigate the impact of navigational data inaccuracies and effects of electromagnetic interaction between the antenna and the aircraft hull. Those were interferometric calibration (improving interferometric co-registration, i.e. reducing trajectory errors) polarimetric calibration and tomographic calibration (enabling 3D focusing). Additionally, ground steering was applied to have the ground response appear at 0 m height in the TomoSAR data, with reference to a Digital Elevation Model (DEM) derived from the lidar Digital Terrain Model (DTM) used to process the SLC images. The DEM was further refined through tomographic processing by the method developed in [26]. The interferometric and tomographic calibration algorithms had to be modified to account for the BS acquisition mode. Care was taken to maintain the same intensity as the original images after refocusing. At L-band the decision was made to not use information from the corner reflector, due to it being located in very near range and was partly affected by residual de-focusing.

Tomographic processing puts high demands on the precision of the flight trajectory estimation error, where calibration is equivalent to estimating the position of the antenna phase center in all passes and target elevation at each range bin [25], [27]. The phase calibration procedure applied for the TomoSense data is essentially the Phase Center Double Localization (PCDL) algorithm, which tackles this problem [25]. The BS L-band data required two phase centers to be estimated, due to the fact that transmitter and receiver locations are different. This was solved by using the MS L-band phase center estimates for the transmitter and only solving for the BS receiver position, which was possible since the MS and BS data were acquired simultaneously.

Regarding radiometric calibration, three identified radiometric unbalances were corrected for: the presence of bias in SLC images, a ground range intensity trend and bias in different headings at L-band. First, some SLC images were seen to be affected by an intensity bias, which was particularly evident at L-band. Minor variations were also observed at P-band. The P-band images were corrected based on the signal from the trihedral reflectors, while at L-band the variation was compensated for by scaling the images such that their average intensities were the same.

The quality of tomographic calibration of TomoSense data was already discussed in our previous publication in [22], which ensured that accurate phase calibration had been accomplished. Regarding radiometric calibration, the TomoSAR products are calibrated within each frequency band, polarization and NW/SE heading. For each such tomogram there is an unknown offset in dB from the true reflectivity of the scene. Furthermore, uncertainties in the antenna radiation pattern at P-band made coverage below 1.4 km ground-range considered unusable. Unfortunately, this region coincides with most of

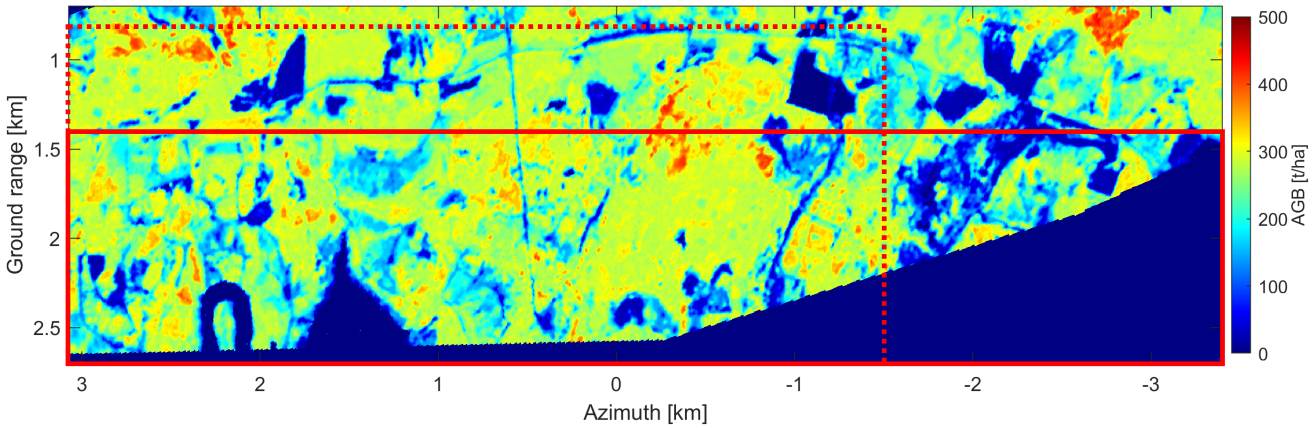

Fig. 2. ALS estimated AGB map, within the coverage of the P- and L-band acquisitions. The solid and dotted red rectangles mark the area used for P-band and covered by L-band respectively.

TABLE I
FRACTION OF FIVE OF THE MOST COMMON FOREST TYPES OVERLAPPED BY BOTH SAR AND ALS.

Forest type	P NW	P SE	L NW	L SE
Beech	35 %	44 %	38 %	48 %
Spruce	34 %	28 %	28 %	25 %
Mixed oak-beech	6 %	4 %	7 %	5 %
Mixed beech-coniferous	6 %	1 %	7 %	1 %
Oak	2 %	4 %	2 %	3 %

the in-situ collected plots, which locations are shown in Fig. 1. Therefore the in-situ plots were not used directly for the TomoSAR analysis in this paper. Also, due to uncertainties in the radiometric quality of the SW data set caused by RFI, only the NW data set was analysed herein.

B. In-situ data and airborne lidar scanning maps

A large scale biotype inventory was done by WuH in 2013 and compiled into a map, where many different forest types can be separated spatially. Forest types include e.g. beech, spruce, pine, oak, coniferous, deciduous and numerous mixed types. There are 38 different forest types present in the area covered by the SAR images. The fraction of five of the most common forest types in the coverage by the NW and SE SAR acquisitions and the ALS are summarized in Table I. It is clear that a majority of the data covers beech and spruce forest. When extracting the beech and spruce forest types, all mixed forest types (i.e., even those mainly containing beech or spruce) are excluded.

CzechGlobe carried out two ALS flights over the Kermeter area; first on the 1st of July 2018 and later a repetition on the 17th of June 2021. The acquisitions resulted in products such as a digital elevation model (DEM), a canopy height model (CHM) and an AGB map of the area. By inspecting the lidar CHM, the mean forest height is about 20 m with a standard deviation of 5.7 m. The maximum canopy height is 43 m.

The AGB maps were processed similarly to, and supported by data from, a previous study in the Silesian Beskids, Czech Republic [28]. The ALS AGB map from the 2021 flight, within the coverage of the P- and L-band SAR images, is shown in Fig. 2. The AGB from ALS was modelled using the Area-Based Approach (ABS) [29], where AGB is represented at a grid-cell level with spatial resolutions of typically 20 m to 30 m [30]. In short, the method uses the 3D point cloud to characterize the ground surface and the vegetation layers above [31], where the vegetation layers are used to calculate discrete metrics related to vegetation properties. The metrics are parameters of the ALS height distribution, e.g. mean and percentiles of the canopy penetration rates (density of lidar echoes from a certain depth). They are used as variables in the models, which are combined with co-located in-situ measured plots [32], [33]. A more thorough description of the ALS processing steps for computing the AGB map is provided in [28].

The final ALS AGB map (partly shown in Fig. 2) shows an R^2 of 0.95 and an RMSE of 27 t/ha when compared to all Kermeter plots. If only comparing it to the test data plots, it shows an R^2 of 0.83 and an RMSE of 48 t/ha. This gives an indication of the expected accuracy. Furthermore, it means that if the TomoSAR AGB retrieval is using the ALS AGB map as a reference and acquires an RMSE around 30 t/ha or lower, then TomoSAR might be more sensitive to AGB than ALS and/or strongly correlated to the metrics used for ALS AGB estimation, causing similar systematic errors. This is important to keep in mind when evaluating performance.

III. METHODOLOGY

A. Data extraction and vertical reflectivity profiles per AGB

The TomoSAR data vectors, where each contain the average Vertical Reflectivity Profile (VRP) over a 0.5 ha area, were extracted and their characteristics and AGB dependence analysed. In the process of extracting VRPs, all maps were averaged over a 0.5 ha area (72 m in ground range and 70.5 m in azimuth). Namely, the VRP $I(z)$ is computed as the intensity of the complex reflectivity $\hat{r}(z)$, as understood from Eq. 2, i.e.

$$I(z) =< |\hat{r}(z)|^2 >, \tag{3}$$

where $< \cdot >$ denotes the average over a 0.5 ha area at height z and parallel to ground level. Biotype masks of forest types

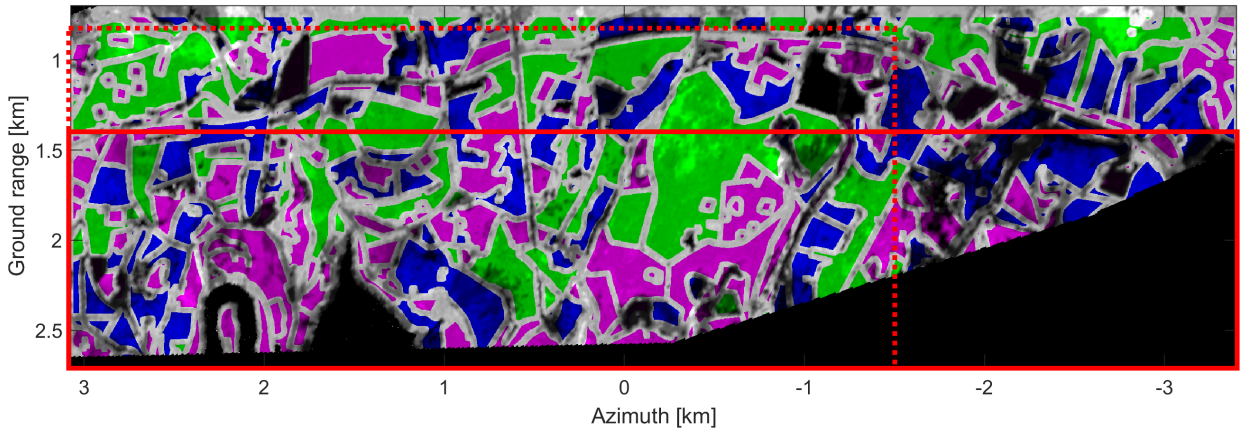

Fig. 3. A biotype segmentation map over the area covered by the P- and L-band acquisitions, with the ALS AGB map in the background scaling the intensity. The areas of extracted data vectors for spruce forest and beech forest are shown in blue and green respectively, while the combined temperate forest also includes the magenta areas. The solid and dotted red rectangles mark the area used for P-band and covered by L-band respectively.

were extracted from the biotype inventory map. The data was filtered such that a margin of 36 m, i.e. half a cell width, was removed around the edge of each forest type region, to make sure that the averaging cell would not mix across borders of forest types. The forest type mask is shown in Fig. 3. VRP data vectors were extracted using a uniform grid with a spacing of 72 m in ground range and 70.5 m in azimuth. Due to suspected radio interference in the SE track SAR images, this study was limited to the NW dataset.

The following method was applied to qualitatively analyse the AGB dependence of the TomoSAR VRPs. The data vectors were sorted into sets of similar AGB values, using 20 tons/ha intervals, and the average VRP of each set was computed. This resulted in a vertical profile curve for each AGB set and the AGB dependence can be analysed from these curves. The AGB dependence is illustrated in the figures by colour mapping the profiles curves.

B. Forest biomass retrieval methods

This study considers three methods based on the exponential model (or power law relationship) relating TomoSAR intensity and AGB. This model has been shown widely applicable and was used extensively in previous radar AGB retrieval studies [17], including P- and L-band TomoSAR [8], [9], [11] for boreal and tropical forest. That is, a function for AGB retrieval is acquired by fitting training data to the model

$$\hat{B} = e^{a_0 + a_1 I_{dB}}, \tag{4}$$

with parameters a_0 and a_1, input intensity (depending on retrieval method) in dB I_{dB} and the resulting AGB estimate $\hat{B}$.

The different methods are ways to compute the intensity I_{dB} from the VRPs. The performance of methods that provide normalized metrics, i.e. that can be compared between data sets without absolute radiometric calibration, is of particular interest to assess due to simplified applicability. The following three methods are studied.

1) Total intensity: The metric is the mean total vertical intensity integral. The results using this metric represent approximately those expected using a traditional multi-look 2D SAR system. The method computes the intensity as

$$I_{tot} = \int_{-\infty}^{\infty} I(z)dz. \tag{5}$$

2) Canopy intensity: The metric is the mean vertical intensity integral over the 20 m to 30 m height span. The main purpose is to reduce the ground backscatter, which is known to reduce retrieval performance. The method computes the intensity as

$$I_c = \int_{20}^{30} I(z)dz. \tag{6}$$

This is similar to the analysis of the 30 m layer for tropical forest in [11], which was the layer of highest AGB correlation in that study. In [8], [9], the 10 m to 30 m layer was used when observing boreal forest. The optimal lower height threshold is varying for different study sites, depending on forest species/structure and tomographic height resolution.

3) Canopy-to-total intensity ratio: The metric is the ratio of the canopy intensity integral to the total intensity integral. This is a normalized metric since any absolute intensity scaling factor cancels out. The method computes the intensity as

$$I_{cr} = \frac{\int_{20}^{30} I(z)dz}{\int_{-\infty}^{\infty} I(z)dz}. \tag{7}$$

The purpose is that this is a slightly more robust metric than the other possible metrics such as the volume-to-ground ratio (VGR), or ground-to-volume ratio (GVR), which is an observable that has been shown sensitive to forest height structure [18], [34]. The argument is that larger trees (a denser forest) would cause more attenuation of the signal reaching the ground, thereby a reduced ground backscatter would be correlated with larger trees. Although, the dependence is not that simple and these metrics are prone to fluctuate for low ground backscatter, as for L-band in a dense (high AGB) forest, or for topographic variations, as for P-band with a generally large ground backscatter (sensitive to ground slope

and double bounce). In comparison, the canopy-to-total ratio is less sensitive to the ground intensity contribution and relies more on reduction of the backscatter return from the canopy below 20 m height with increasing AGB. This provides robustness and forest height sensitivity since the canopy backscatter below 20 m height is significant (see Fig. 4).

C. Training, validation and retrieval performance metrics

There are numerous ways to approach performance analysis of forest AGB retrieval methods. The simplest choice is to use all data samples for both model training and validation, i.e. to estimate model parameters and to evaluate performance. The problem with this approach is obviously that the estimated model parameters are dependent on the same data that the model is evaluated on. Consequently, the resulting estimates are often too optimistic [35]. To acquire more realistic results, (ideally) independent data sets should be used for model training and validation respectively [35]. An optimal setup would be to acquire training and validation data from different sites, although representing the same AGB range, species composition and topography. If such conditions are not fulfilled or the area of measurement and reference data is limited to a single site, the data need to be partitioned. This approach opens up for many combinations of training/validation sets of the data samples, also e.g. by choosing the sets such that the AGB range is similar or by using the best quality reference data for validation. Additionally, data subsets can be cross-validated on each other and the average performance evaluated [35]. An example of this iterative procedure is the "leave-one-out" method, where each data point is estimated and validated by using all other data points for training.

For this analysis, the data vectors were sorted in increasing AGB where every 2nd data vector was chosen for model training and the remaining data vectors were used for model validation. A crucial part of any parameter retrieval analysis is to present comparable performance metrics that represent the applicability of the methods. It is most common in studies to use the coefficient of determination R^2, the Root-Mean-Squared Error (RMSE) and the relative RMSE (RMSE %), i.e. the percentage of the RMSE to the mean AGB, to evaluate method performance (see e.g. [8], [9], [11]).

The coefficient of determination R^2 goodness-of-fit metric is defined as [36]

$$R^2 = \frac{\sum_{i=1}^{N}(\hat{B}_i - \mu_B)^2}{\sum_{i=1}^{N}(B_i - \mu_B)^2}, \tag{8}$$

where B are reference AGB values, $\hat{B}$ are estimated AGB values and μ_B is the mean reference AGB. N is the number of data samples evaluated. This statistic describes the fraction of the variance of B that is captured in the model estimate $\hat{B}$. With reference to the litterature review in Section I.A, an R^2 in the range 0.5 to 0.7 would be considered good and values above that would be outstanding. In turn, the RMSE is defined as

$$\text{RMSE} = \sqrt{\frac{1}{N}\sum_{i=1}^{N}(B_i - \hat{B}_i)^2}, \tag{9}$$

and it describes the level of absolute error of the model estimates $\hat{B}$ to the reference AGB B. The relative RMSE is then

$$\text{RMSE } \% = \frac{\text{RMSE}}{\mu_B}, \tag{10}$$

which is is a statistic describing the relative error.

It is also common to include the estimation bias among performance metrics, which is not considered in this study. This is due to all areas being about equally represented in the training and validation data, which means that the bias is purely caused by the ratio of the variability that is not explained by the model. I.e., an R^2 less than 1 implies weight being added to the mean of the training data, causing a bias, and an R^2 of 0 results in the model only guessing on the mean of the training data (only a bias). Therefore, information on the bias is not seen to add substance to the analysis.

D. Evaluation of ground slope nuisance

A ground surface normal can be parameterized by using two spherical angles describing the slope and aspect of the surface relative to zenith and azimuth [37]. The ground slope angle is denoted u and defined as the angle between zenith and that of the ground-plane normal, while the aspect angle, denoted v, is the angle between azimuth and the projection of the ground-plane normal onto the azimuth-ground-range plane. In this study, only the ground slope angle u is used for the analysis. The nuisance effect of the ground slope is simply evaluated by conditioning the data on three levels of ground slope: 1) all ground slopes (i.e. $u < 90°$), 2) ground slope angles $u < 20°$ and 3) ground slope angles $u < 10°$. The TomoSAR AGB training and validation procedure is performed on the set of data fulfilling each condition and the results are compared.

IV. Vertical Reflectivity Profiles

The average Vertical Reflectivity Profile (VRP) of each AGB set is shown in Fig. 4 for P- and L-band MS and BS NW track acquisitions at HH, HV and VV polarization. Fig. 4a-4c show the result for the two main forest types in the area; spruce and beech forest. Fig. 4d also shows the resulting MS mode VRPs dependence on AGB for temperate forest in general, a combination of all forest types. The AGB sets consist of the VRPs of the data vectors sorted into 20 t/ha intervals, where each curve is coloured from blue (low AGB, minimum 80 t/ha) to red (high AGB, maximum 400 t/ha) according to the colour scale shown in the figure. Samples are more scarce, especially for beech forest, at low AGB (below about 200 t/ha) and therefore the average VRPs from those AGB intervals originate from fewer data vectors. Thus, the uncertainty due to possible local variations should be kept in mind.

A relationship between radar backscatter intensity and AGB has long been observed, but only for either SAR backscatter or for methods making use of some "arbitrary" height interval (often significantly limited by vertical resolution), see Section I-A for TomoSAR examples. Fig. 4 is a way of directly observing the AGB dependence of the intensity as a function of height. Then, one can motivate why a certain height interval would work well for AGB retrieval using some kind of

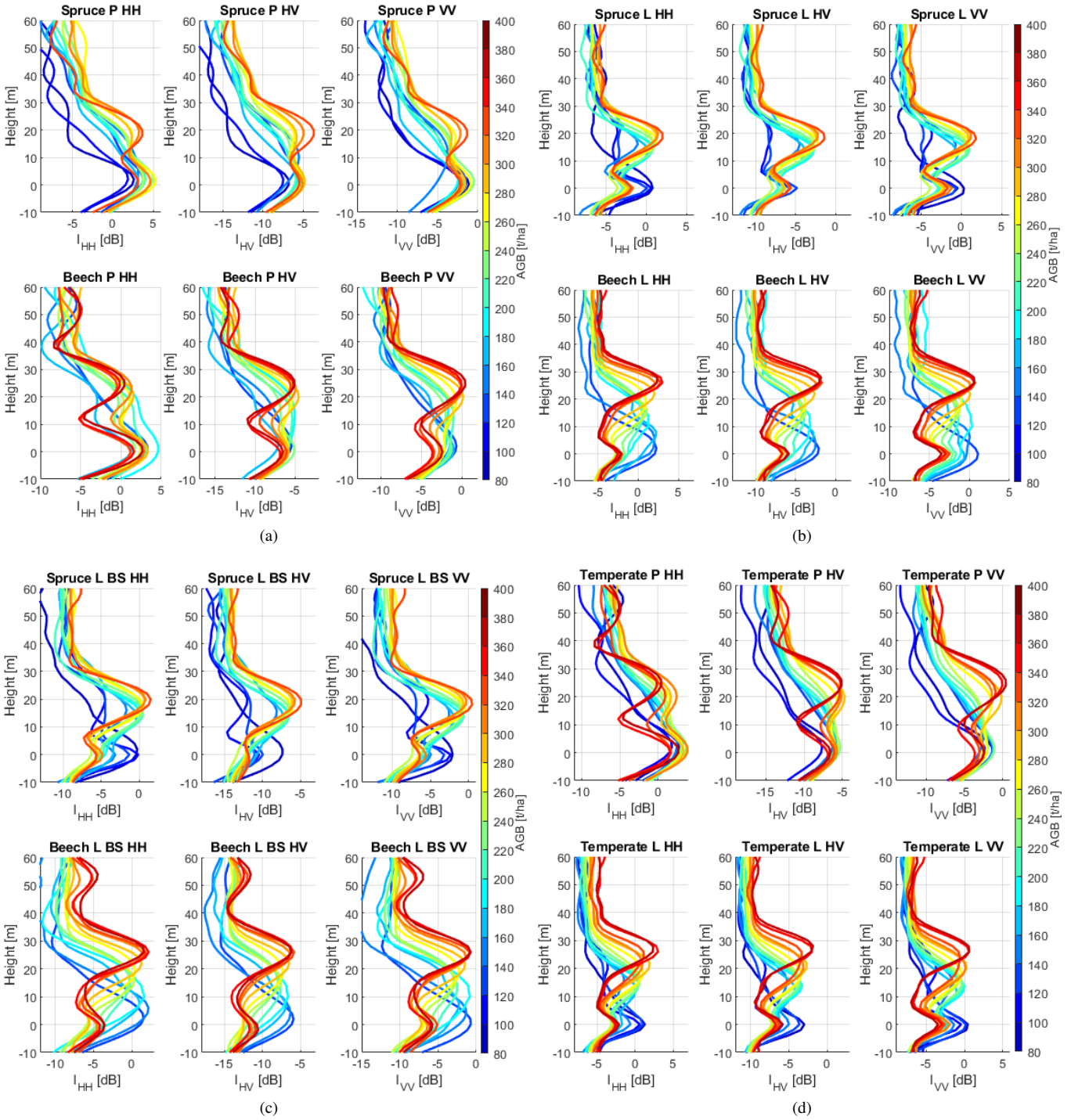

Fig. 4. Average vertical reflectivity profiles within 20 t/ha AGB intervals observed at P- and L-band. Mono-static (MS) mode results for the spruce and beech forest types are shown in (a) and (b), while bi-static (BS) mode is shown in (c). The MS mode result for temperate forest in general, a combination of all forest types, is shown in (d). There is an undetermined offset in the dB scales within each frequency band and polarisation relative to absolute reflectivity.

monotonically increasing model, such as Eq. 4. Of course, Fig. 4 shows the AGB dependence at the landscape level, where stand level variations are present due to structural and presumably dielectric differences. Such differences will result in unexplained variance when fitting e.g. Eq. 4.

In general, a clear dependence on AGB for the VRPs is observed. A larger AGB is connected to a larger portion of the intensity being located at a height about 10 to 30 m above ground, with the height of maximum intensity in this interval increasing with AGB. This behavior is expected since a larger forest biomass would imply more, higher and thicker trees, presumably also with more branches, contributing to the backscattered intensity. There is also the ground reflection clearly seen at 0 m height, overall (but not necessarily) decreasing with increasing AGB. It decreases more rapidly with AGB at L-band than at P-band, where the decrease is

most apparent at VV polarization in beech forest. At L-band it is about equally apparent for all polarizations in the beech forest, while the ground reflection at HV polarization in spruce forest show the least dependence on AGB. The observation of a decreasing ground reflection component is expected since the signal is subject to more attenuation when propagating through a thicker forest media and that shorter wavelengths (higher frequencies) are more sensitive to smaller structures; presumably located mainly in the canopy. This is also the reason why the L-band profiles are expected to have a larger portion of the observed intensity originating from the upper canopy and have a more similar polarization dependence than the P-band profiles.

The VRPs of the spruce and beech forest types show a different AGB dependence. Spruce forest profiles grow strongly in intensity with AGB and slightly in height, as is seen when one compares the VRPs above about 260 t/ha (yellow to red curves). Beech forest profiles grow strongly in height but not in intensity. However, note that the AGB of the beech forest is in general higher than that of the spruce forest. Such a difference in AGB dependence can be speculated to originate from the forest type structure. A spruce tree typically has many branches distributed along a large portion of its height, also with some decrease of branch size near the top. As the spruce tree grows, it is reasonable to assume that the number and size of branches along the tree increases. Thus, the total backscatter could increase, and not only be shifted upwards as the tree grows or the forest becomes denser (i.e. an increase in AGB). This explains the strong intensity and weaker height dependence of the spruce forest vertical profiles. In contrast, a (larger) beech tree typically has most of its branches spreading around its top. A beech forest can be quite airy, with a few branches distributed along its trunks (containing a majority of its AGB) below the upper canopy. As the beech forest grows, it is speculated that its density and number of branches does not increase significantly, but mainly be elevated in height. This could explain the stronger height dependence of the beech forest vertical profiles.

In more detail, the three polarizations show different characteristics from which a number of qualitative observations on the AGB dependence can be done. This is most apparent at P-band (Fig. 4a), where the spruce forest profiles at HH show a large variance in profile evolution with AGB, especially for the ground peak. In contrast, HV shows a considerably more stable ground peak and the profile demonstrate a significant growth of total intensity with AGB as the canopy peak steadily increases. At VV the total intensity is not as obviously sensitive to AGB as the ground peak is slightly attenuated and the canopy peak is not as strongly increasing with AGB as for HV. In terms of spruce forest AGB retrieval prospects, P-band total intensity methods show AGB sensitivity especially at HV. Additionally, the canopy peak height and intensity or profile phase center indicate a promising AGB sensitivity.

P-band beech HH profiles show a less clear dependence on AGB, apart from the elevation and slight reduction of the canopy peak. At HV the profile evolution is considerably clearer. It is interesting to note that the intensity peak is about constant for all profiles while the ground peak does not change much. In turn, at VV the profile evolution is also clear, while the canopy peak is slightly increasing and the ground peak decreasing with increasing AGB. This suggests that P-band non-tomographic SAR intensity methods would not show much sensitivity to beech forest AGB. Rather, the canopy peak and height or profile phase center is expected to convey AGB information.

In the L-band spruce profiles (Fig. 4b and 4c) the ground peak is seen to first decrease and then increase again with AGB. This is more apparent for the MS than the BS acquisition mode. It is noted that this effect originates from higher AGB spruce forest (in this dataset) being located at flatter terrain. More specifically, 72 % of the spruce data vectors with more than 300 t/ha AGB are located at ground slopes smaller than 10°. In comparison, the corresponding ratio for spruce data vectors with less than 300 t/ha AGB is 39 % and for below 260 t/ha it is 30 %. Due to this the ground-trunk double-bounce reflection can be more pronounced for high AGB spruce forest. The profiles are similar on all polarizations, with a clear evolution in both height and intensity of the canopy peak. If anything, HV show a slightly more rapid canopy peak intensity increase with AGB than HH and VV. The relative ground peak for low AGB is also smaller than that seen in HH and VV. Regarding spruce forest AGB retrieval methods at L-band: AGB sensitivity is expected in the canopy peak height and especially intensity or profile phase center.

The L-band beech profiles show a clear evolution with AGB. They are almost identical at all polarizations, with the only difference that the ground peak is slightly larger at VV (and HH for BS mode) than at HV. The total intensity contribution from the canopy peak and the ground peak, each increasing and decreasing correspondingly, seem to add up to approximately a constant. Again, even clearer than for P-band, L-band non-tomographic SAR intensity methods are not expected to show sensitivity to beech forest AGB. However, the height of the canopy peak is expected to provide AGB information.

Observing the average reflectivity profiles of the temperate forest (a combination of all 38 forest types), there is a clear transition for both the P- and L-band profiles from low to high AGB at 20 m to 30 m height, as is seen in Fig. 4d. The intensity grows steadily throughout this region, which means that it can provide significant information of the forest AGB. The temperate forest average profile show more variance in its evolution with AGB than the ones separate for spruce and beech, which indicate that a segmentation of forest types will improve AGB sensitivity. At L-band, the maximum of the intensity in the interval is growing slightly more in height than at P-band. Again, as for spruce and beech forest separately, this can be an expected behavior.

Comparing the reflectivity profiles seen for L-band MS and BS acquisitions, it can first be said that they look similar. The curves are almost identical for all polarizations and forest types, above a height of 5 m above ground. Below 5 m height is where the difference show up, where the ground reflection is slightly less prominent for medium to high AGB (above about 180 t/ha) in the BS data. It can be speculated that this is caused by a reduced double-bounce reflection between the

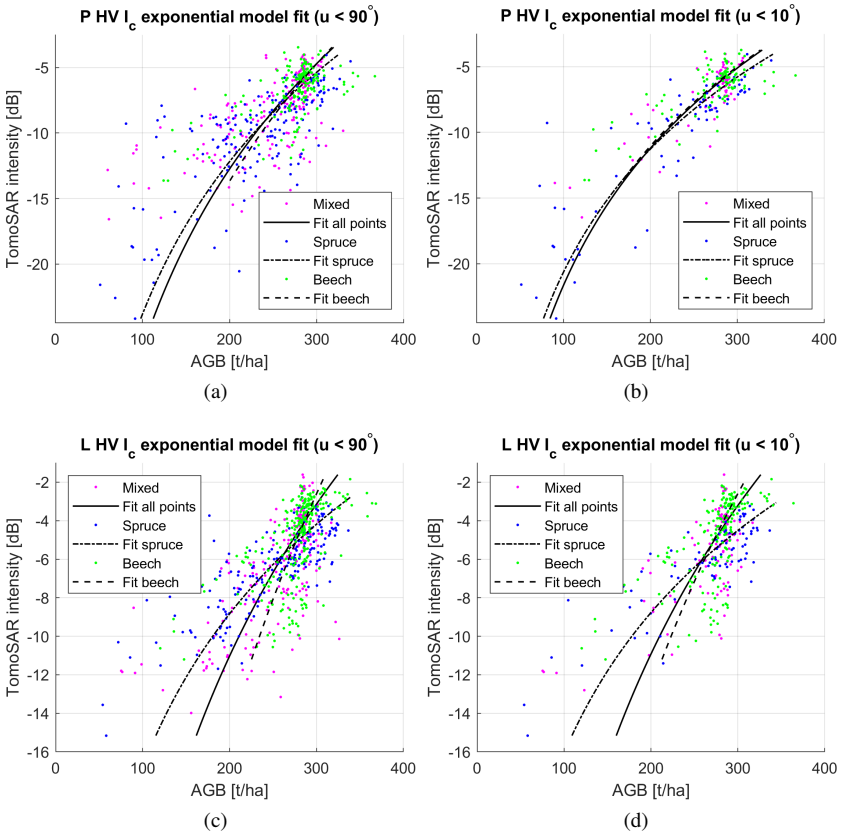

Fig. 5. Exponential model fit curves for P- and L-band HV canopy (20-30 m height layer) intensity to ALS AGB, for all ground slope angles (i.e. $u < 90°$) in (a) and (c) and for ground slope angles $u < 10°$ in (b) and (d). There is an undetermined offset in each dB scale relative to absolute reflectivity.

tree trunk and the ground in the direction of the receiver in the BS mode. Furthermore, a computation of the SNR, as the intensity range from the VRP's maximum to their noise floor (approximated as the mean intensity level at 40 m to 60 m height), for all data vectors show a 2.2 dB, 0.1 dB and 2.0 dB larger mean SNR at HH, HV and VV respectively for the BS data.

V. Forest Biomass Retrieval

A. Exponential model fit evaluation

The observed TomoSAR canopy intensity I_c, i.e. 20 to 30 m height intensity integral, of each data vector is compared with its ALS AGB value, as is shown in Fig. 5 for the HV polarization at P- and L-band. An exponential model is fitted to the clusters of points, on the form of Eq. 4. The corresponding curves for each forest type are included in Fig. 5a to 5d, where Fig. 5b and 5d only includes data points that satisfy the ground slope angle condition $u < 10°$. The exponential model fit curves for P-band in Fig. 5a are practically identical for the different forest types. When limiting the ground slope angle in Fig. 5b, the model fits are essentially unchanged while the variance of the points around the fit is clearly reduced. In the L-band data of Fig. 5c the model fits are more varying between forest types. Compared to the temperate forest type, the model fit tilt is increased for spruce forest and decreased for beech forest. This is an indication that the AGB dependence is changing for the forest types when transitioning from P-band to L-band. The L-band model fits do not show any significant change when limiting the ground slope to $u < 10°$, as is seen in Fig. 5d. The effects are similar for HH and VV, for both I_{cr} and I_{tot}. I.e., for less sloping areas there is a reduced variance around the model fit at P-band.

It is noted that a linear model fit actually outperforms the exponential model fit in terms of RMSE and R^2 for the cases presented in this study. The performance difference is not very significant, in terms of RMSE about 0.5 to 2 t/ha (where absolute RMSE is in the range of 20 to 50 t/ha), but it is systematic. The reason why there is no gain in using an exponential model fit for this data set may be the relatively high AGB of the observed forest. Previous studies have found it matching "low" AGB well, typically below 100 t/ha [2], [8], [9]. This data set has only 10-15 data points below 100 t/ha AGB, which is less than 3 % of the total set. Still, the decision was made to use the exponential model, since that is the standard of previous work on direct SAR AGB retrieval [17].

B. TomoSAR AGB retrieval performance

The resulting HV polarization P- and L-band MS TomoSAR AGB retrievals for spruce and beech forest using the three methods are shown in Fig. 6-8. The first method is using the total VRP intensity integral I_{tot} (total intensity) as input to the model described in Eq. (4). I_{tot} corresponds to the backscatter in a multi-looked SAR image. The second method is using the

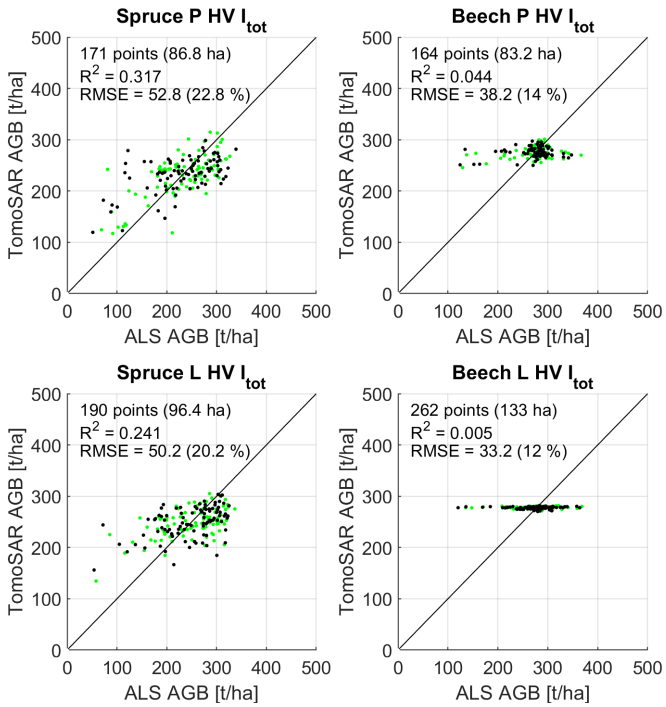

Fig. 6. TomoSAR AGB retrieval using the total intensity, corresponding to the backscatter in a SAR image. Training points are shown in green and validation points in black. The L-band data is for mono-static mode.

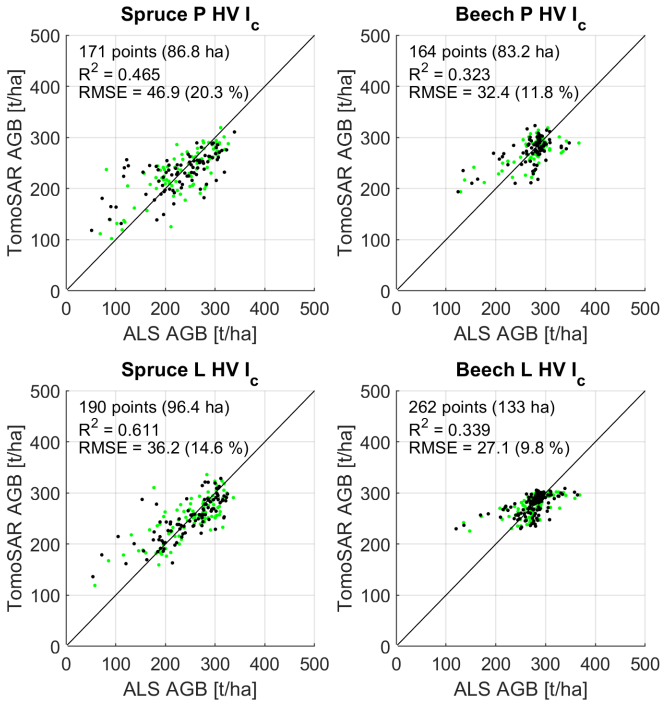

Fig. 7. TomoSAR AGB retrieval using the canopy intensity integral. Training points are shown in green and validation points in black. The L-band data is for mono-static mode.

20 to 30 m height integral of the VRP I_c (canopy intensity), as this height region in general indicates high sensitivity to AGB in Fig. 4. The third method is the ratio of the first two $I_{cr} = I_c/I_{tot}$ (canopy-to-total intensity ratio), providing a normalized metric. The resulting R^2, RMSE and % of RMSE referenced to the mean AGB of the data points are summarized in Tables II-IV for P-band, L-band MS and L-band BS acquisitions respectively. A general temperate forest type is also included in the tables, which is the result obtained using all forest type data points without discrimination. The number of data points given in the tables are the total number of data points used for both training (50 %) and validation (50 %).

It is worth mentioning that the spread of AGB affects R^2. Therefore, it can be lower for beech forest than for spruce forest, while at the same time the beech forest RMSE is smaller than that of the spruce forest. The R^2 is in general higher for spruce forest, which is partly due to the AGB being more evenly distributed. The presence of a bias centered around the mean AGB is expected for R^2 values less than 1, as was explained in Section III-C. At low correlation the AGB estimate tends to approach its mean, as this is the best it can do. The TomoSAR AGB retrieval plot would then look flat for the data points. Due to this, the RMSE of a method completely uncorrelated to beech forest AGB can still be lower than that of a method which show correlation to spruce forest AGB. Also keep in mind that the topography of the Kermeter area is quite hilly, more so than many of the areas covered in other radar forest studies, which influences the results (especially for P-band). This matter is given attention in the next section, see Tables V-VI. Also, the observed VRP

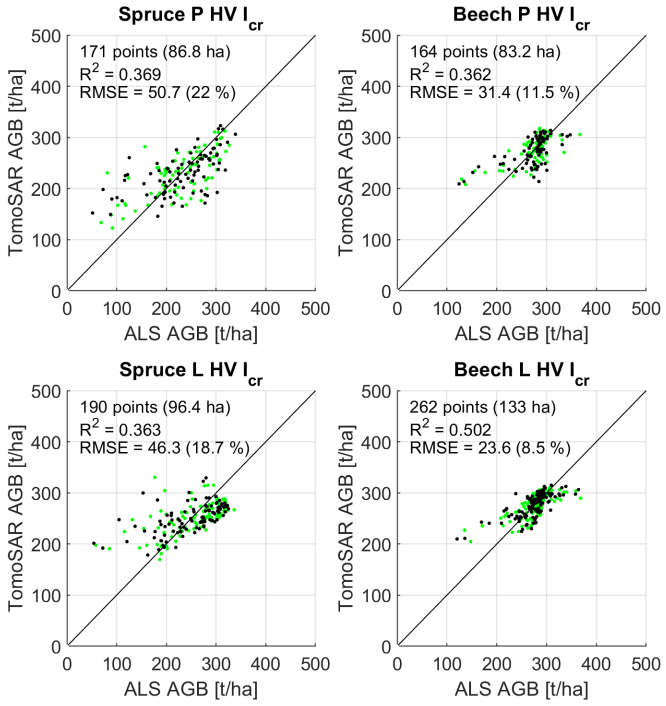

Fig. 8. TomoSAR AGB retrieval using the canopy-to-total intensity ratio. Training points are shown in green and validation points in black. The L-band data is for mono-static mode.

AGB dependence presented in the previous section provides important information on how to interpret the performance of different AGB retrieval methods and they will be continuously referred to.

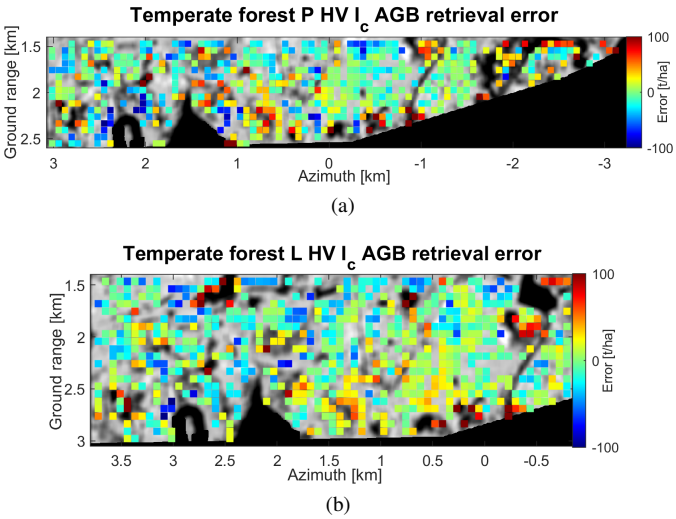

Fig. 9. Temperate forest AGB retrieval error maps for P- and L-band HV canopy intensity, shown in (a) and (b) respectively, on top of a gray scale ALS AGB map for position reference. The areas include both training and validation data and the colour scale spans from -100 to 100 t/ha.

1) Total intensity method: The total intensity I_{tot} for P-band spruce forest is significantly more sensitive to AGB at HV than at HH and VV. This corresponds well to what has been seen in previous studies, such as [38]. The resulting R^2 is 0.32 and the RMSE is 52.8 t/ha (22.8 %). Similar results are seen for MS L-band spruce forest, with an R^2 of 0.24 at HV being the strongest . Interestingly, the results for beech forest are quite different. With an R^2 of 0.01-0.10 the I_{tot} is essentially uncorrelated to beech forest AGB. This is the case at all polarizations and even clearer so for L-band. The temperate forest results for I_{tot} at P-band show something in between those of spruce and beech forest separately; there is a very low R^2 of 0.09 at HH, the strongest R^2 of 0.31 at HV and an R^2 of 0.25 at VV, which is much larger than that of either spruce or beech forest. The VV results may indicate a different response from mixed forest types than that of a single-species forest, or from some of the species present in the mixed forest (e.g. oak or pine). The results for L-band temperate forest are clearly different, much like those for beech forest, with almost no correlation to AGB.

2) Canopy intensity method: When instead observing the canopy intensity I_c, as seen in Fig. 7, the gains of using TomoSAR compared to SAR is clear. AGB information contained in the vertical distribution of reflectivity is now made use of. As a result, all AGB retrieval performance metrics are significantly improved compared to those using I_{tot}, especially at HH and VV. P-band spruce forest results show an R^2 of 0.47 and an RMSE of 46.9 t/ha (20.3 %) at HV, while HH and VV show almost identical sensitivity with an R^2 of 0.36 and 0.35 respectively. The difference is even more pronounced for spruce forest at L-band, with an R^2 of 0.61 and 0.68 and RMSE of 36.2 (14.6 %) and 33.4 (13.5 %) for MS and BS mode respectively. A similar but slightly weaker performance is seen for HH and VV, where R^2 ranges between 0.56-0.62. Thus, for spruce forest the sensitivity at L-band is similar for all polarizations.

The I_c for beech forest radically changes the AGB sensitivity compared to I_{tot}. At P-band, VV show the strongest R^2 of 0.41 and with an RMSE of 30.5 t/ha (11.2 %). Sensitivity is apparent at HV with an R^2 of 0.32, but much less so at HH with an R^2 of 0.10. This corresponds well to what is indicated in the VRPs of Fig. 4a, where the canopy reflectivity at VV grows the strongest with AGB while at HH it shows more variance and even reduces slightly for high AGB. The results for beech forest at L-band are similar at all polarizations, with an R^2 of 0.34 and RMSE of 27.1 t/ha (9.8 %) at HV for MS mode and an R^2 of 0.39 and RMSE of 26.1 t/ha (9.4 %) at VV for BS mode.

The temperate forest I_c results at P-band interestingly show a stronger R^2 than what is seen for spruce and beech forest separately, with an R^2 of 0.53 and an RMSE of 37.7 t/ha (15.0 %) at HV and similar at VV. At HH a weaker R^2 of 0.35 is observed. At L-band, again, all polarizations show similar retrieval performance. The R^2 is 0.43 and with an RMSE of 35.7 t/ha (13.6 %) for HV MS mode and the BS mode sensitivity is just barely better. Error maps of the temperate forest P- and L-band I_c AGB retrieval are shown in Fig. 9.

3) Canopy-to-total intensity ratio method: The third and last method evaluated is the canopy-to-total ratio I_{cr}, for which spruce and beech forest results at P- and L-band HV are shown in Fig. 8. The performance for spruce forest is in general weaker than that of the canopy intensity I_c, which may be explained by the normalization procedure neglecting the AGB information contained in the absolute intensity. It was argued in the previous section, by inspecting the VRPs in Fig. 4, that a significant part of the spruce forest AGB sensitivity is contained in the absolute intensity. This is also indicated by the total intensity R^2 for spruce HV in Fig. 6 at both P- and L-band. For spruce forest at P-band, the I_{cr} performance is similar at HV and VV with an R^2 of 0.39 and an RMSE of 50.1 t/ha (21.7 %) at VV. A slightly weaker sensitivity is seen at HH. For L-band, it can be noted that the HH polarization now show the strongest sensitivity with an R^2 of 0.40 and an RMSE of 45.1 t/ha (18.2 %) for MS mode and an R^2 of 0.54 and an RMSE of 39.5 t/ha (15.9 %) for BS mode. The HV and VV performance is just slightly weaker.

Beech forest I_{cr} results do for all cases in Tables II-IV show a better performance compared to those of I_c. It is speculated that since the beech forest I_{tot} is seen almost completely insensitive to AGB, the intensity normalization does (unlike for spruce) not reduce AGB sensitivity. On the contrary, it might remove absolute intensity nuisance variations and thereby explain the improvement. Also, when inspecting the beech forest VRPs of Fig. 4 the ground peak at both P- and L-band is overall decreasing with AGB. The inverse AGB dependence of the ground peak part of I_{tot} would then support the total AGB sensitivity of the increasing I_c in the ratio $I_{cr} = I_c/I_{tot}$. Although, local variations of the ground peak can also be a nuisance factor. The beech forest P-band results show the strongest sensitivity at VV, with an R^2 of 0.46 and an RMSE of 29.5 t/ha (10.8 %). HV show a slightly lower R^2 of 0.36 and HH an R^2 of 0.26, which has improved the most compared to that of I_c. At L-band, the results are similar for all polarizations and acquisition modes. BS mode

TABLE II
P-BAND TOMOSAR AGB RETRIEVAL PERFORMANCE METRICS.

Forest type	Method P MS	HH [R^2, RMSE (%)]	HV [R^2, RMSE (%)]	VV [R^2, RMSE (%)]	Data points
Spruce	I_{tot}	0.16, 58.5 (25.4)	0.32, 52.8 (22.8)	0.08, 62.4 (27.0)	171
	I_c	0.36, 51.4 (22.3)	0.47, 46.9 (20.3)	0.35, 51.6 (22.3)	
	I_{cr}	0.32, 52.7 (22.8)	0.37, 50.7 (22.0)	0.39, 50.1 (21.7)	
Beech	I_{tot}	0.01, 38.9 (14.2)	0.04, 38.2 (14.0)	0.10, 37.2 (13.6)	164
	I_c	0.10, 37.5 (13.7)	0.32, 32.4 (11.8)	0.41, 30.5 (11.2)	
	I_{cr}	0.26, 33.9 (12.4)	0.36, 31.4 (11.5)	0.46, 29.5 (10.8)	
Temperate	I_{tot}	0.09, 52.7 (21.0)	0.31, 45.8 (18.2)	0.25, 47.7 (19.0)	531
	I_c	0.35, 44.7 (17.8)	0.53, 37.7 (15.0)	0.51, 38.8 (15.4)	
	I_{cr}	0.47, 40.6 (16.1)	0.48, 39.9 (15.9)	0.51, 38.6 (15.4)	

TABLE III
L-BAND MONO-STATIC (MS) TOMOSAR AGB RETRIEVAL PERFORMANCE METRICS.

Forest type	Method L MS	HH [R^2, RMSE (%)]	HV [R^2, RMSE (%)]	VV [R^2, RMSE (%)]	Data points
Spruce	I_{tot}	0.15, 53.3 (21.5)	0.24, 50.2 (20.2)	0.21, 51.1 (20.1)	190
	I_c	0.58, 37.3 (15.0)	0.61, 36.2 (14.6)	0.56, 38.2 (15.4)	
	I_{cr}	0.40, 45.1 (18.2)	0.36, 46.3 (18.7)	0.32, 47.7 (19.2)	
Beech	I_{tot}	0.00, 33.2 (12.0)	0.01, 33.2 (12.0)	0.00, 33.3 (12.0)	262
	I_c	0.32, 27.4 (9.9)	0.34, 27.1 (9.8)	0.29, 28.2 (10.2)	
	I_{cr}	0.48, 24.0 (8.7)	0.50, 23.6 (8.5)	0.51, 23.5 (8.5)	
Temperate	I_{tot}	0.01, 44.8 (17.1)	0.07, 45.6 (17.4)	0.03, 46.3 (17.7)	663
	I_c	0.42, 35.9 (13.7)	0.43, 35.7 (13.6)	0.38, 37.0 (14.1)	
	I_{cr}	0.46, 34.8 (13.3)	0.45, 34.8 (13.3)	0.42, 35.8 (13.6)	

TABLE IV
L-BAND BI-STATIC (BS) TOMOSAR AGB RETRIEVAL PERFORMANCE METRICS.

Forest type	Method L BS	HH [R^2, RMSE (%)]	HV [R^2, RMSE (%)]	VV [R^2, RMSE (%)]	Data points
Spruce	I_{tot}	0.07, 55.9 (22.5)	0.22, 50.9 (20.5)	0.19, 51.9 (20.9)	190
	I_c	0.60, 36.7 (14.8)	0.68, 33.4 (13.5)	0.62, 35.4 (14.3)	
	I_{cr}	0.54, 39.5 (15.9)	0.44, 43.5 (17.5)	0.47, 42.3 (17.1)	
Beech	I_{tot}	0.02, 33.0 (11.9)	0.01, 33.1 (12.0)	0.01, 33.1 (12.0)	262
	I_c	0.39, 25.9 (9.4)	0.34, 27.0 (9.8)	0.39, 26.1 (9.4)	
	I_{cr}	0.49, 23.7 (8.6)	0.49, 23.8 (8.6)	0.53, 22.9 (8.3)	
Temperate	I_{tot}	0.06, 46.1 (17.6)	0.08, 45.4 (17.3)	0.02, 46.7 (17.8)	663
	I_c	0.45, 34.8 (13.3)	0.46, 34.7 (13.2)	0.45, 35.0 (13.4)	
	I_{cr}	0.54, 31.9 (12.2)	0.50, 33.3 (12.7)	0.52, 32.8 (12.5)	

VV show an R^2 of 0.53 and an RMSE of 22.9 t/ha (8.3 %). The BS mode I_{cr}, unlike for I_c, shows no improvement at any polarization compared with the MS mode results.

The results for temperate forest I_{cr} are in general similar or slightly improved compared to those seen for I_c, with all polarizations having a similar performance. At P-band, the only significant improvement is seen at HH, such that it is comparable to HV and VV. At VV an R^2 of 0.51 and an RMSE of 38.6 t/ha (15.4 %) is observed. For L-band at HH, an R^2 of 0.46 and an RMSE of 34.8 t/ha (13.3 %) is seen for MS mode and for BS mode the R^2 is 0.54 with an RMSE of 31.9 t/ha (12.2 %).

4) Mono- and bi-static mode comparison: A comparison of the performance seen for the L-band MS and BS acquisitions shows that, in general, the BS mode tends to improve the results slightly. The most significant differences between the modes are seen for spruce I_{cr} HH and VV, beech I_c VV and temperate I_{cr} HH and VV, where R^2 is increased in the range of 0.08-0.15 compared to MS mode. It can be noted that the two modes show a very similar performance for beech forest I_{cr}. The only case where the MS mode might be performing better is for spruce forest I_{tot} HH, but that is rather irrelevant due to the low R^2 of 0.15. The differences are speculated to originate from two main factors: SNR and scattering mechanics. As mentioned in the previous section, the span of the VRPs in intensity from the noise floor to their maximum is about 2 dB larger for the BS mode at HH and VV,

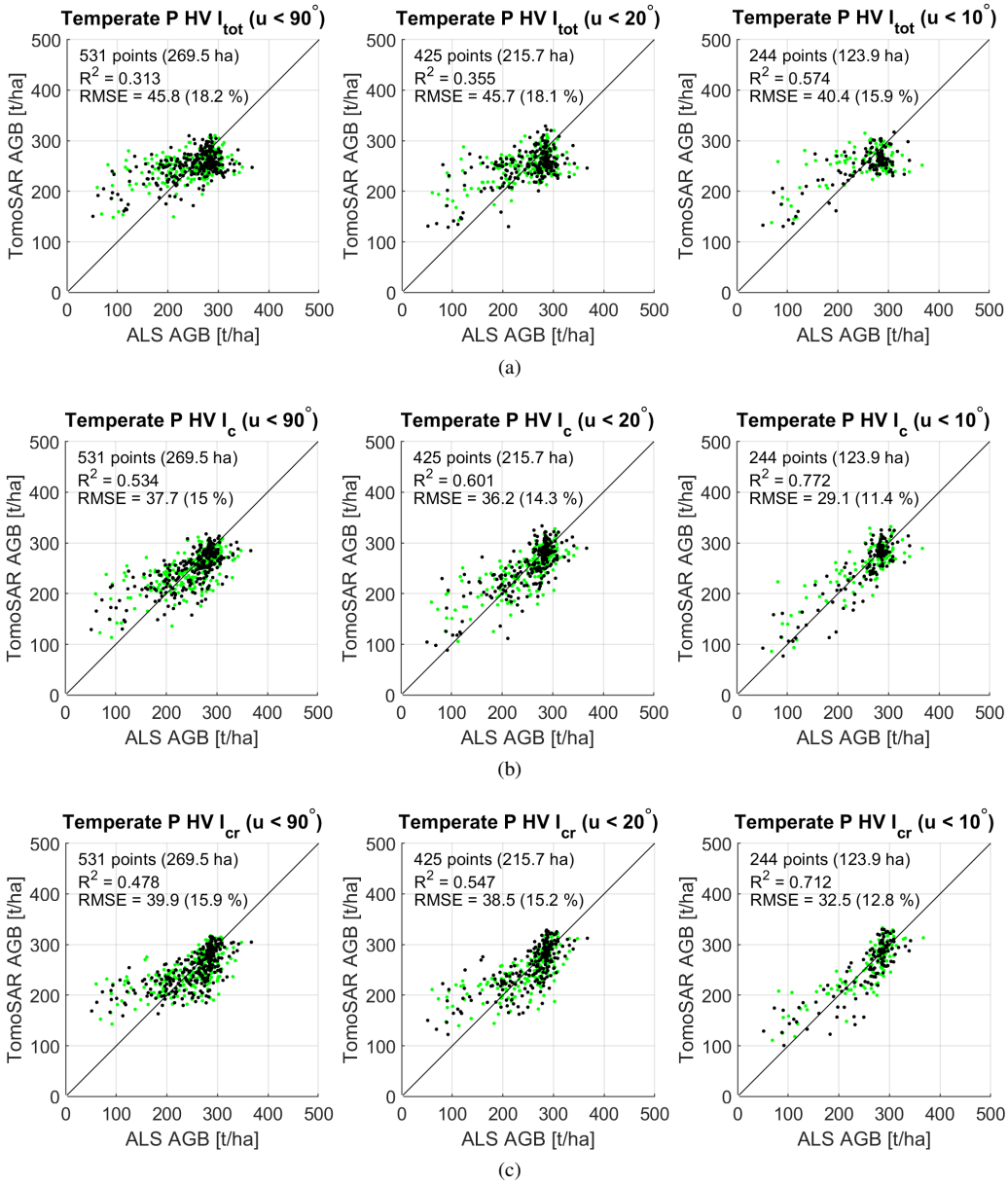

Fig. 10. P-band TomoSAR temperate forest AGB retrieval for (a) the total intensity method, corresponding to SAR image backscatter, (b) the canopy intensity method and (c) the canopy ratio method, with data points conditioned on the ground slope angle u.

which indicates a better SNR in the sense of the methods here used for AGB retrieval. Regarding the scattering, the BS mode show a weaker (or even no noticeable) increase of the ground peak for high AGB spruce forest, while that is apparent for the MS mode (see Fig. 4). This can explain the differences seen for spruce and temperate forest. For beech forest, the ground peak of the VRPs is reduced for medium AGB in the BS mode and especially at VV, which also reduces its leakage into the I_c region at 20 m to 30 m height. This may explain the slight improvement. For the I_{cr} case where the modes show equal results, it can similarly be noted that the BS mode ground peak is not monotonically decreasing with AGB, while it is for MS mode. This effect can cancel out the improvement that would otherwise be expected due to the better SNR.

VI. Ground slope nuisance factor

The area covered by the radar acquisitions have quite some topographic variations, with ground slopes up to $37°$ within the analysed set of data. This makes a good opportunity to study the influence of ground slope on the performance of the AGB retrieval methods. At P-band 54 % of the data points are located at a ground slope larger than $10°$ and 20 % on a ground slope of more than $20°$. Correspondingly at L-band, 45 % of the data points are located at a ground slope larger than $10°$ and 16 % at more than $20°$. Fig. 10-11 show the AGB retrieval performance of the three retrieval methods at P- and L-band temperate forest HV when conditioning the data points on three different ground slope angles, denoted by u. The conditions are $u < 90°$ (i.e. use all data points), $u < 20°$ and $u < 10°$. The performance metric results (R^2, RMSE and RMSE in % relative to mean AGB) for the spruce, beech and

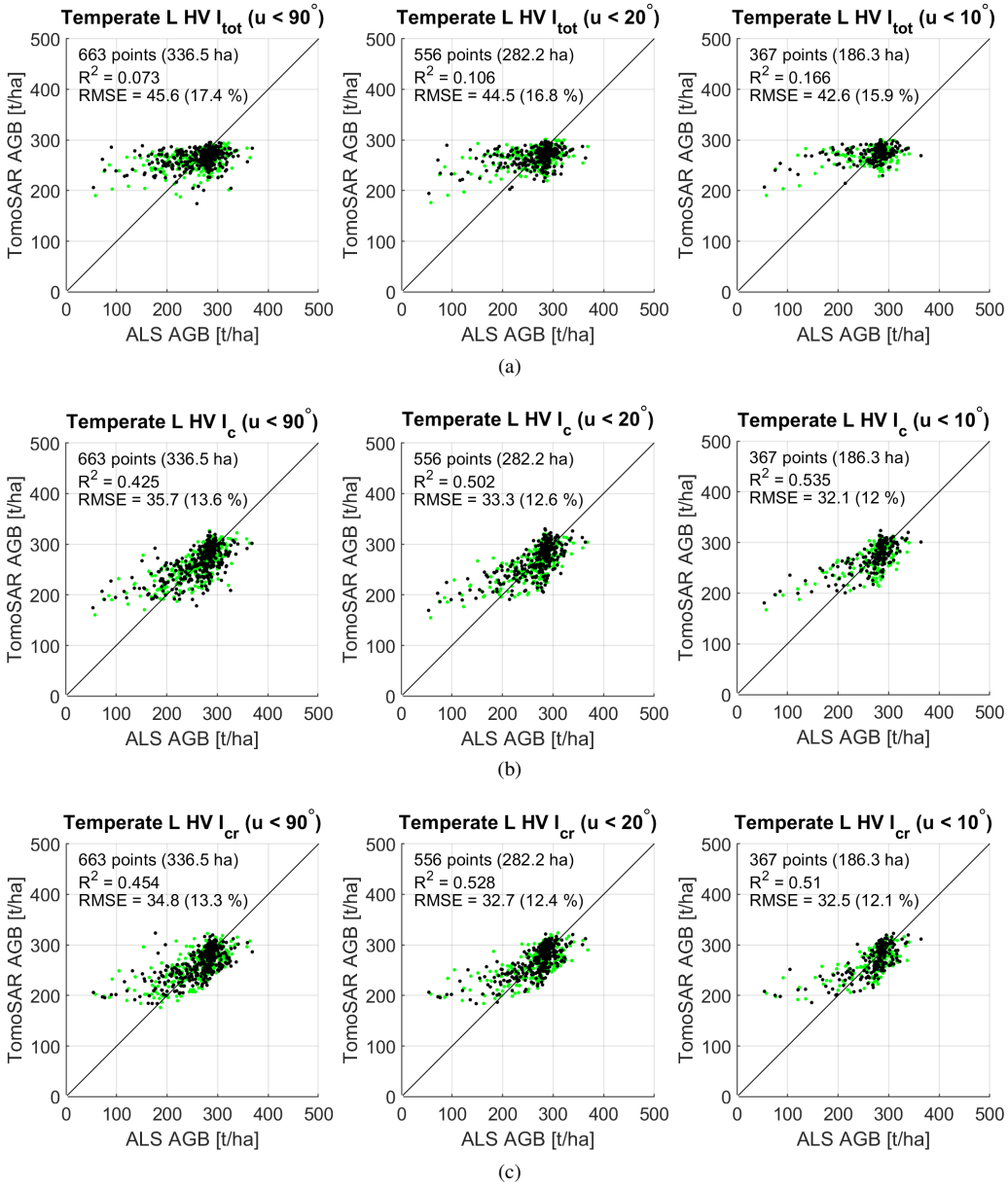

Fig. 11. L-band mono-static TomoSAR temperate forest AGB retrieval for (a) the total intensity method, corresponding to SAR image backscatter, (b) the canopy intensity method and (c) the canopy ratio method, with data points conditioned on the ground slope angle u.

temperate forest types at HV and for each of the three AGB retrieval methods, for each condition, are compiled in Tables V-VI. The number of data points given in the tables are, as in the previous section, the total number of data points for both training and validation.

In general, the ground slope angle is seen to have a significant impact on the P-band AGB retrieval performance. At L-band, the ground slope angle shows an influence on the spruce forest AGB performance metrics, but not so much for the beech and temperate forest. Even if the R^2 is increased the RMSE does not show an as clear improvement, an effect due to a reduced bias in the AGB estimation for low AGB while the variance of the points tend to increase slightly. The model fit minimizes the MSE (thus also the RMSE) for the points given, which in general is expected to increase when reducing the number of points used. Note that when conditioning the data points on a ground slope angle of $u < 10°$ there are still 244 data points composing the temperate forest P-band results, covering a total area of 124 ha. At L-band the corresponding number of data points is 367, covering an area of 186 ha. This makes the temperate forest observations the strongest indicator of the slope nuisance effect presented in this analysis. The BS mode results show a similar behaviour as those for the MS mode, in general with a slight performance improvement.

A. Nuisance for the total intensity method

Observing the total intensity I_{tot} at HV, spruce forest P-band results show an R^2 of 0.52 when the ground slope $u < 20°$ and an R^2 of 0.64 for $u < 10°$. The R^2 performance metric is doubled when limiting the ground slope to $10°$, greatly improving AGB sensitivity even for I_{tot}. At L-band, the spruce

TABLE V
SUMMARY TABLE OF P-BAND MONO-STATIC HV SLOPE NUISANCE FACTOR.

Forest type	**Method P MS HV**	$u < 90°$ [R^2, RMSE (%)]	$u < 20°$ [R^2, RMSE (%)]	$u < 10°$ [R^2, RMSE (%)]	**Data points**
Spruce	I_{tot}	0.32, 52.8 (22.8)	0.52, 48.5 (21.3)	0.64, 48.8 (21.7)	171, 140, 73
	I_c	0.47, 46.9 (20.3)	0.64, 41.1 (18.1)	0.86, 35.1 (15.6)	
	I_{cr}	0.37, 50.7 (22.0)	0.51, 46.4 (20.4)	0.80, 40.0 (17.8)	
Beech	I_{tot}	0.04, 38.2 (14.0)	0.05, 39.4 (14.5)	0.02, 46.2 (17.0)	164, 144, 99
	I_c	0.32, 32.4 (11.8)	0.44, 30.3 (11.1)	0.52, 32.1 (11.8)	
	I_{cr}	0.36, 31.4 (11.5)	0.50, 29.1 (10.7)	0.68, 26.2 (9.7)	
Temperate	I_{tot}	0.31, 45.8 (18.2)	0.36, 45.7 (18.1)	0.57, 40.4 (15.9)	531, 425, 244
	I_c	0.53, 37.7 (15.0)	0.60, 36.2 (14.3)	0.77, 29.1 (11.4)	
	I_{cr}	0.48, 39.9 (15.9)	0.55, 38.5 (15.2)	0.71, 32.5 (12.8)	

TABLE VI
SUMMARY TABLE OF L-BAND MONO-STATIC (MS) HV SLOPE NUISANCE FACTOR.

Forest type	**Method L MS HV**	$u < 90°$ [R^2, RMSE (%)]	$u < 20°$ [R^2, RMSE (%)]	$u < 10°$ [R^2, RMSE (%)]	**Data points**
Spruce	I_{tot}	0.24, 50.2 (20.2)	0.30, 51.7 (20.7)	0.40, 49.4 (18.9)	190, 153, 87
	I_c	0.61, 36.2 (14.6)	0.65, 35.9 (14.4)	0.75, 32.7 (12.5)	
	I_{cr}	0.36, 46.3 (18.7)	0.48, 43.6 (17.4)	0.62, 39.5 (15.1)	
Beech	I_{tot}	0.01, 33.2 (12.0)	0.02, 33.9 (12.3)	0.00, 37.0 (13.5)	262, 240, 177
	I_c	0.34, 27.1 (9.8)	0.44, 25.7 (9.3)	0.42, 28.4 (10.4)	
	I_{cr}	0.50, 23.6 (8.5)	0.54, 23.2 (8.4)	0.55, 25.2 (9.2)	
Temperate	I_{tot}	0.07, 45.6 (17.4)	0.11, 44.5 (16.8)	0.17, 42.6 (15.9)	663, 556, 367
	I_c	0.43, 35.7 (13.6)	0.50, 33.3 (12.6)	0.54, 32.1 (12.0)	
	I_{cr}	0.45, 34.8 (13.3)	0.53, 32.7 (12.4)	0.51, 32.5 (12.1)	

forest results show a similar, but less pronounced, behavior. The R^2 increases from 0.24 to 0.40 when limiting the data points to ground slopes below $10°$. The beech forest total intensity I_{tot} P-band results are still completely insensitive to AGB when limiting the ground slope angle. This is also the case at L-band. Temperate forest I_{tot} P-band R^2 of originally 0.31 does not show much change when limiting to $20°$ (R^2 is then 0.36), but a significant improvement to 0.57 for $10°$ limit. For L-band, the sensitivity is improved from almost none to a weak R^2 of 0.17.

B. Nuisance for the canopy intensity method

The impact of ground slope on the canopy intensity I_c performance is considerable at P-band. Spruce forest HV results are improved from an R^2 of 0.47 and RMSE of 46.9 t/ha (20.3 %) to an R^2 (the highest in this paper) of 0.86 and RMSE of 35.1 t/ha (15.6 %) when limiting the ground slope angle to below $10°$. At L-band an improvement is seen from an R^2 of 0.61 to 0.75, which is significant, while not as strong as that seen for P-band. For beech forest at P-band R^2 increases steadily form 0.32 to 0.44 for $u < 20°$ and then to 0.52 for $u < 10°$. The RMSE does not change much. As previously mentioned, this can be expected due to the reduced number of data points. L-band beech forest I_c only shows a slight improvement when limiting the ground slope angle to $20°$, while the results doesn't change to the better for lower limits. This indicates a different dependence than for spruce forest. Temperate forest P-band AGB retrieval performance is improved from an R^2 of 0.31 and an RMSE of 45.8 t/ha (18.2 %) to an R^2 of 0.77 and an RMSE of 29.1 t/ha (11.4 %) when limiting the ground slope angle. At L-band the effect is less prominent, with R^2 increasing slightly from 0.43 to 0.54.

C. Nuisance for the canopy-to-total intensity ratio method

There is also a clear effect on I_{cr} AGB retrieval performance due to the ground slope at the data points. For spruce forest P-band the AGB sensitivity changes strongly when limiting the ground slope angle. R^2 goes from 0.37 to 0.80 and the RMSE from 50.7 t/ha (22.0 %) to 40.0 t/ha (17.8 %). At L-band there is still a significant improvement for spruce forest performance, with R^2 increasing from 0.36 to 0.62. Beech forest P-band results show a significantly improved AGB sensitivity compared to that of I_c when limiting u. The metrics change from an R^2 of 0.36 and an RMSE of 31.4 t/ha (11.5 %) to an R^2 of 0.68 and an RMSE of 26.2 t/ha (9.7 %). The results for the L-band beech forest data are quite different. There is almost no improvement seen when neglecting larger ground slopes. The temperate forest P-band performance steadily improves when limiting u. The R^2 changes from 0.48 to 0.71 and the RMSE from 39.9 t/ha (15.9 %) to 32.5 t/ha (12.8 %). For temperate forest L-band results, only a slight improvement is seen for $u < 20°$, but even less for $u < 10°$.

VII. Further discussion

A. Forest AGB information from vertical reflectivity profiles

It is apparent from the reflectivity profiles, as was presented in Fig. 4, that they inhabit a significant dependence on AGB, which also is different for spruce and beech forest. The total backscatter was seen to increase with AGB for spruce, but not for beech. As was speculated in Section IV, the differences might be explained by the forest structure of the tree species, where a typical spruce tree often has a larger number of branches (scatterers) distributed more evenly along its height than those of a typical beech tree. Previous work has been done on deriving forest structure descriptors from TomoSAR profiles, see e.g. [13], [39]. In those studies, absolute radiometric information was discarded since the input for the structure estimators was the height distribution of backscatter peaks in the VRP. It would be interesting to assess how well forest structure descriptors are able to capture the differences between forest types, if it changes their relationship to AGB and if radiometric information can add to their quality.

The full information on AGB embedded in the average VRPs is most certainly not captured by the first order power-law relationship over a fixed height integral, as is used for AGB retrieval in this study. Although, it might be the case that the VRPs inherent variability due to nuisance factors such as forest texture, speckle noise, incidence angle and ground response limits the quality of information to a similar level even with more sophisticated analysis methods. Such methods could rely e.g. on modeling of the backscatter or by statistically characterizing the expected shape and variations of the VRP with AGB.

B. TomoSAR forest AGB retrieval performance

1) Comparisons: L-band TomoSAR AGB retrieval using empirical relations to forest structure was done for a study in Traunstein [16]. It covered a temperate forest site with dominant spruce forest, where HH/HV showed an R^2 of 0.77/0.72 and RMSE of 38/43 t/ha (19/21 %) under dry conditions. The ground slope of the area is up to 10° and the results are similar to those at L-band HV for spruce forest in this study when limiting the ground slope, with an R^2 of 0.75 and RMSE of 33 t/ha (13 %). If just considering the RMSE, they are also similar to that of the temperate forest type (32 t/ha at L-band HV). Thus the performance of the direct and empirical structure relation approaches may be similar, but the topographic influence on the structure method performance is yet to be assessed. AGB retrieval by L-band TomoSAR was also evaluated over a boreal site in [9]. With an R^2 of 0.67, the results were similar to those here obtained for spruce forest using the canopy intensity method with an R^2 of 0.61-0.75. The main differences are the significantly higher average AGB of the forest, the larger ground slopes, the use of the 20 m to 30 m height layer (rather than the 10 m to 30 m height layer) and the considerably better vertical resolution in this study [9]. Compare e.g. the less than 5 m vertical resolution (30 flight tracks) in the TomoSense L-band data with the 15 m vertical resolution (5 flight tracks) in the Traunstein study [16].

P-band temperate forest TomoSAR AGB retrieval has not been done in other studies, which limits comparisons of the results. However, the spruce forest results can be compared with those in boreal sites. Retrieval for the BioSAR-1 and -2 datasets was analysed in [8], noting an R^2 of 0.50-0.70 and an RMSE of 27-33 t/ha (30-36 %) for HV. In comparison, the sensitivity seen in this study is significantly greater when limiting the ground slope to below 10 °, especially for spruce forest. If not limiting the ground slope, the results are comparable. That is, overlooking that the average AGB is much higher in the Kermeter site and thus the relative RMSE lower. The vertical resolution in this study is also considerably better [8].

2) Limitations: A relevant consideration is to what extent the TomoSAR AGB retrieval performance evaluated in this paper is limited by the reference AGB. Similar studies have been able to make use of in-situ plot measurements of forest structure and with AGB estimates less uncertain than those of the ALS AGB map used in this study. At the same time, some of the here shown TomoSAR AGB performance results obtained using the ALS AGB map as a reference shows a similar uncertainty as that of the reference itself. This leads to the conclusion that, even with the simple retrieval method applied in this study, the performance is most likely limited by the reference uncertainty. Any observations of TomoSAR AGB retrieval below about 30 t/ha RMSE would be due to a better adaptation to the systematic error of the ALS estimates (with an RMSE of 27 t/ha), which makes it hard to draw conclusions of the actual AGB sensitivity in such a case.

3) Improvements: A few approaches to improve the AGB retrieval can be considered. First, combinations of polarimetric channels in the TomoSAR retrieval of tropical forest AGB was evaluated for P-band in [12], but a purely HV based method outperformed all such methods. It is thus not apparent that polarimetric combinations could improve the AGB estimates, but it should be further investigated. The study also showed that a second-order model might improve the performance slightly, while here only a first-order model was evaluated. Another prospect is of course to combine observations at different frequency bands, as has been studied for P- and L-band PolInSAR over boreal forest in [40]. One of the best performing methods made use of the L-band HV backscatter in combination with the P-band HH/VV ratio. This relies on the strong relationship between ground-trunk double-bounce and AGB seen for P-band, which may not be as beneficial for TomoSAR, especially in sloping terrain. However, it is a subject with potential to further improve AGB estimates.

Furthermore, it has been observed that boreal and tropical forest AGB retrieval using direct backscatter in general is improved when combined with a forest height parameter, estimated from TomoSAR or PolInSAR [12], [40]. Judging from the apparent vertical profile height dependence on AGB seen in Fig. 4, it would be surprising if this is not the case also for the TomoSense dataset. Thus, another prospect for improved AGB retrieval is to apply a method incorporating a TomoSAR forest height estimate. It would also be of interest to evaluate forest structure relation approaches such as the one used in the Traunstein study [16], especially for the

strong topography of the Kermeter area. Lastly, the differences for forest types seen in this study support the possibility of improving total AGB estimates by using different parameters or models depending on forest type.

4) Nuisances: A significant topographic nuisance is present even when removing the ground response. Areas of large ground slope and areas of large local incidence angle overlap. It can be argued which one of these is dominating the nuisance effect, but conditioning on the ground slope angle yields improved results. In practice, the effect is probably due to a combination of several biophysiological, radio wave propagation/scattering and TomoSAR processing factors. To comment on the improvement observed for P-band but not for L-band in Fig. 10 and 11, one can speculate that a larger part of the P-band canopy peak originates from scatterers further down the canopy layers (larger structures) than that of L-band (smaller structures and more attenuated). The P-band canopy peak might then be affected more by a larger propagation distance through the canopy to the main scatterers than that of the L-band canopy peak. In addition to this, the main structures contributing to the L-band backscatter intensity might simply not be as strongly coupled to AGB as those for P-band. With this said, it is not apparent how to draw any direct conclusions about the physical origin of the ground slope nuisance factor from these results, which is out of the scope of this study.

In addition to the Kermeter site, Krycklan (Sweden) and Nouragues (French Guiana) are two reasonably hilly sites imaged by TomoSAR, covering boreal and tropical forest, respectively [8], [9], [11]. The significantly better vertical resolution in TomoSense (5 to 15 m at P-band, compared to 21 to 104 m in BioSAR-2 and about 20 m in TropiSAR) allows for a unique analysis of the vertical distribution of reflectivity, as was done in this study. Further analysis of ground slope effects and related mitigation methods done jointly on these three data sets to cover boreal, temperate and tropical forests, e.g. in the settings of spaceborne missions such as BIOMASS, is left for future work.

Another nuisance factor is the dielectric variation in the scene, both spatially and temporally. E.g., dry or moist conditions (after rain) was seen to affect TomoSAR AGB sensitivity at L-band [16]. It has also been observed that both P- and L-band VRPs in a boreal forest can vary more than 1 dB over a day, hypothesized to be caused by tree water content variations and transpiration phenomena [41], [42]. Transpiration activity in temperate forests is greater than in boreal forests [43]. Soil moisture variations are also an apparent factor affecting the ground response and possibly the dielectric properties of trees. However, the influence of these effects on TomoSAR AGB retrieval remain uncertain.

5) Needs: As an answer to the need for improved mapping of global biomass, the main goal for the BIOMASS mission is to monitor forest AGB with an error of less than 20 % or 10 t/ha [2], [3]. The performance of AGB retrieval in this study consistently shows relative RMSE values within that limit, by applying the simple first-order power law relationship. More sophisticated methods can most certainly improve the retrieval performance. This study thereby shows that P- and L-band TomoSAR is well suited for large scale temperate forest AGB monitoring, which makes an important addition to the results of previous ESA campaigns over tropical forest (TropiSAR and AfriSAR) and boreal forest (BioSAR-1 and -2) [19], [44]–[49]. Although, a challenge for BIOMASS, as a global mission, is to acquire enough high-quality training data to fulfill the AGB estimation error specification [3]. Another possibility is to use the sparse satellite-based lidar AGB estimates acquired by Global Ecosystem Dynamics Investigation Lidar (GEDI) and ICESat-2 (Ice, Cloud, and Land Elevation Satellite 2) as reference data, but the effect on performance is uncertain [50]. This approach has been simulated for the L-band NASA-ISRO SAR (NISAR) mission in [51]. It may also be possible to combine L-band NISAR observations with P-band BIOMASS observations to further improve AGB estimates [3].

VIII. Conclusion

As a part of the TomoSense ESA campaign, Tomographic Synthetic Aperture Radar (TomoSAR) was applied to image the 3D reflectivity of a temperate forest located in the Kermeter area of Eifel National Park in North Rhine-Westphalia, Germany. The test site consisted of dominant beech and spruce forest, which provided a unique opportunity to study these two species separately, in addition to temperate forest in general. The topography is pronounced, with many ground slopes in the range of 20-40 °, allowing for the analysis of ground slope effects. Data vectors each covering a 0.5 ha area are studied, 531 at P-band and 663 at L-band (both MS and BS modes), for HH, HV and VV polarizations. An Airborne Lidar Scanning (ALS) derived Above-Ground Biomass (AGB) estimation map is used as a reference for the sensitivity assessment. The ALS estimation show an R^2 of 0.95 and an RMSE of 27 t/ha compared to in-situ forest plot AGB estimates.

Vertical Reflectivity Profile (VRP), i.e. backscatter, observations show a clear AGB dependence, with characteristics depending on forest type. A high AGB is connected to a large portion of the intensity being located at a height about 10 m to 30 m above ground, with the height of maximum intensity in this interval increasing with AGB. This behavior is expected since a large forest biomass would imply many, tall and thick trees, often with large branches, contributing to the backscattered intensity. The main difference between the species is that spruce VRPs grow strongly in intensity and slightly in height with AGB, while beech VRPs grow strongly in height but not in intensity. This behaviour is speculated to originate from the forest structure, where a large spruce tree typically contain a larger number of branches distributed along its height, thereby increasing its backscatter intensity, while a large beech tree often have a fairly constant number and size of branches located at the very top as it grows in height, hence not increasing its backscatter intensity. This has an impact on AGB retrieval, since vertical resolution is found necessary to estimate beech forest AGB. The 20 to 30 m height interval consistently show an increasing intensity for increasing AGB in the average VRPs, indicating that it is well suited for AGB retrieval using a monotonically increasing mapping function.

TomoSAR AGB retrieval is done by directly mapping intensity to AGB using an exponential model, trained on 50 %

of the data. The performance is evaluated for three methods: total intensity integral I_{tot}, representing performance without vertical resolution (such as regular SAR), canopy intensity integral I_c, using the intensity of the 20 to 30 m height layer, and canopy-to-total intensity ratio I_{cr}, which is a normalized metric corresponding to I_c divided by I_{tot}. A linear model actually outperforms the exponential model in terms of both R^2 and RMSE for most cases studied. The improvement is not very significant, about 0.5 - 2.0 t/ha compared to the results presented for the exponential model (in the 20 to 50 t/ha RMSE range). The exponential model was still used for the performance evaluation due to its previous extensive application in SAR AGB retrieval.

Three categories are studied: temperate forest (a combination of all forest types), spruce forest and beech forest. I_{tot} show a sensitivity to spruce AGB at both P- and L-band, especially for HV, which agrees well with observations in previous SAR and TomoSAR studies. No frequency band show any significant sensitivity for beech. In turn, I_c greatly improves the sensitivity. In general, temperate forest at P-/L-band HV show an R^2 of 0.53/0.43 and an RMSE of 38/36 t/ha (15/14 %). Correspondingly, I_{cr} show an R^2 of 0.48/0.45 and an RMSE of 40/35 t/ha (16/13 %). Compared with I_c, spruce AGB sensitivity is reduced at both bands while that of beech is increased, especially at L-band. This emphasizes a dependence on height and low correlation with absolute intensity of beech forest AGB, while spruce forest AGB retrieval perform worse when the absolute intensity information is removed.

The ground slope is shown to be a significant nuisance factor for P-band retrieval performance. When limiting the ground slope angle to below 10 °, the R^2 measure for I_c over temperate forest is improved from 0.53 to 0.77, with the RMSE changing from 38 t/ha (15 %) to 29 t/ha (11 %). The most significant improvement is seen for spruce P-band HV, where R^2 changes from 0.47 to 0.86. Temperate forest using I_{cr} show a similar but slightly weaker improvement as I_c.

Previous research on forest TomoSAR observations have focused on either direct AGB retrieval from height layer intensity integrals, or the estimation of forest structure parameters to be used as input for empirical relations. This paper adds to the knowledge of TomoSAR sensitivity to forest AGB by showing and analysing the AGB dependence of reflectivity profiles and the differences between forest types, i.e. for spruce, beech and general temperate forest. Specifically, beech forest characteristics have not been addressed before in a TomoSAR study, while many (boreal, hemi-boreal and temperate forest) studies have covered mainly spruce forest. The results of the I_{cr} method for AGB retrieval are potentially important, since it shows a similar performance to the absolute canopy intensity method while being a normalized metric, avoiding the challenge of absolute calibration. The topographic ground slope nuisance on the forest AGB retrieval for P-band is well known for SAR, but the still significant nuisance when only observing the canopy intensity with TomoSAR is an important result.

Lastly, none of the AGB retrieval methods studied in this paper are exclusive to TomoSAR. I_{tot} is simply the SAR image backscatter. I_c can be obtained by interferometric SAR, through ground-notching (or notching e.g the 15 m layer) [7], also providing forest height estimates, using way fewer than the 28-30 baselines in the TomoSense campaign. This is beneficial for these AGB retrieval methods, since they can be applied in many SAR settings, but what role remains for TomoSAR? The answer lies in the demands on vertical resolution. TomoSAR remains an important tool for AGB estimation, in terms of understanding the underlying mechanisms that provide information (or nuisance) on AGB, or forest structure and vitality for that matter.

ACKNOWLEDGMENT

We acknowledge support from ESA under ESA/ESTEC contract TOMOSENSE: Technical Assistance for Airborne Measurements during the Tomographic Sensing Experiment, ESA, 4000127285/19/NL/FF/gp.

REFERENCES

[1] R. A. Houghton, F. Hall, and S. J. Goetz, "Importance of biomass in the global carbon cycle," *Journal of Geophysical Research: Biogeosciences*, vol. 114, 6 2009.

[2] T. Le Toan, S. Quegan, M. Davidson, H. Balzter, P. Paillou, K. Papathanassiou, S. Plummer, F. Rocca, S. Saatchi, H. Shugart, and L. Ulander, "The BIOMASS mission: Mapping global forest biomass to better understand the terrestrial carbon cycle," *Remote Sensing of Environment*, vol. 115, pp. 2850–2860, 11 2011.

[3] S. Quegan, T. Le Toan, J. Chave, J. Dall, J.-F. Exbrayat, D. H. T. Minh, M. Lomas, M. M. D'Alessandro, P. Paillou, K. Papathanassiou, F. Rocca, S. Saatchi, K. Scipal, H. Shugart, T. L. Smallman, M. J. Soja, S. Tebaldini, L. Ulander, L. Villard, and M. Williams, "The European Space Agency BIOMASS mission: Measuring forest above-ground biomass from space," *Remote Sensing of Environment*, vol. 227, pp. 44–60, 6 2019.

[4] J. Xiao, F. Chevallier, C. Gomez, L. Guanter, J. A. Hicke, A. R. Huete, K. Ichii, W. Ni, Y. Pang, A. F. Rahman, G. Sun, W. Yuan, L. Zhang, and X. Zhang, "Remote sensing of the terrestrial carbon cycle: A review of advances over 50 years," *Remote Sensing of Environment*, vol. 233, p. 111383, 11 2019.

[5] T. Le Toan, A. Beaudoin, J. Riom, and D. Guyon, "Relating forest biomass to SAR data," *IEEE Transactions on Geoscience and Remote Sensing*, vol. 30, pp. 403–411, 3 1992.

[6] A. Beaudoin, T. Le Toan, S. Goze, E. Nezry, A. Lopes, E. Mougin, C. C. Hsu, H. C. Han, J. A. Kong, and R. T. Shin, "Retrieval of forest biomass from SAR data," *International Journal of Remote Sensing*, vol. 15, pp. 2777–2796, 9 1994.

[7] M. J. Soja, S. Quegan, M. M. d'Alessandro, F. Banda, K. Scipal, S. Tebaldini, and L. M. H. Ulander, "Mapping above-ground biomass in tropical forests with ground-cancelled P-band SAR and limited reference data," *Remote Sensing of Environment*, vol. 253, p. 112153, 2 2021.

[8] E. Blomberg, L. M. H. Ulander, S. Tebaldini, and L. Ferro-Famil, "Evaluating P-band TomoSAR for biomass retrieval in boreal forest," *IEEE Transactions on Geoscience and Remote Sensing*, vol. 59, pp. 3793–3804, 5 2021.

[9] E. Blomberg, L. Ferro-Famil, M. J. Soja, L. M. H. Ulander, and S. Tebaldini, "Forest biomass retrieval from L-band SAR using tomographic ground backscatter removal," *IEEE Geoscience and Remote Sensing Letters*, vol. 15, pp. 1030–1034, 7 2018.

[10] D. H. T. Minh, T. Le Toan, F. Rocca, S. Tebaldini, M. M. d'Alessandro, and L. Villard, "Relating P-band synthetic aperture radar tomography to tropical forest biomass," *IEEE Transactions on Geoscience and Remote Sensing*, vol. 52, pp. 967–979, 2 2014.

[11] D. H. T. Minh, T. Le Toan, F. Rocca, S. Tebaldini, L. Villard, M. Réjou-Méchain, O. L. Phillips, T. R. Feldpausch, P. Dubois-Fernandez, K. Scipal, and J. Chave, "SAR tomography for the retrieval of forest biomass and height: Cross-validation at two tropical forest sites in French Guiana," *Remote Sensing of Environment*, vol. 175, pp. 138–147, 3 2016.

[12] N. Ramachandran, S. Saatchi, S. Tebaldini, M. M. d'Alessandro, and O. Dikshit, "Mapping tropical forest aboveground biomass using airborne SAR tomography," *Scientific Reports*, vol. 13, p. 6233, 4 2023.

[13] M. Pardini, M. Tello, V. Cazcarra-Bes, K. P. Papathanassiou, and I. Hajnsek, "L- and P-band 3-D SAR reflectivity profiles versus lidar waveforms: The AfriSAR case," *IEEE Journal of Selected Topics in Applied Earth Observations and Remote Sensing*, vol. 11, pp. 3386–3401, 10 2018.

[14] D. H. T. Minh, L. Villard, L. Ferro-Famil, S. Tebaldini, and T. Le Toan, "P-Band SAR tomography for the characterization of tropical forests," *2017 IEEE International Geoscience and Remote Sensing Symposium (IGARSS), Fort Worth, Texas, USA*, pp. 5862–5865, 7 2017.

[15] T. Fatoyinbo, J. Armston, M. Simard, S. Saatchi, M. Denbina, M. Lavalle, M. Hofton, H. Tang, S. Marselis, N. Pinto, S. Hancock, B. Hawkins, L. Duncanson, B. Blair, C. Hansen, Y. Lou, R. Dubayah, S. Hensley, C. Silva, J. R. Poulsen, N. Labrière, N. Barbier, K. Jeffery, D. Kenfack, M. Herve, P. Bissiengou, A. Alonso, G. Moussavou, L. T. White, S. Lewis, and K. Hibbard, "The NASA AfriSAR campaign: Airborne SAR and lidar measurements of tropical forest structure and biomass in support of current and future space missions," *Remote Sensing of Environment*, vol. 264, p. 112533, 10 2021.

[16] A. T. Caicoya, M. Pardini, I. Hajnsek, and K. Papathanassiou, "Forest above-ground biomass estimation from vertical reflectivity profiles at L-band," *IEEE Geoscience and Remote Sensing Letters*, vol. 12, pp. 2379–2383, 12 2015.

[17] M. Schlund, K. Scipal, and S. Quegan, "Assessment of a power law relationship between P-band SAR backscatter and aboveground biomass and its implications for BIOMASS mission performance," *IEEE Journal of Selected Topics in Applied Earth Observations and Remote Sensing*, vol. 11, pp. 3538–3547, 10 2018.

[18] S. Tebaldini and F. Rocca, "Multibaseline polarimetric SAR tomography of a boreal forest at P- and L-bands," *IEEE Transactions on Geoscience and Remote Sensing*, vol. 50, pp. 232–246, 1 2012.

[19] I. Hajnsek, M. Pardini, R. Horn, R. Scheiber, K. Papathanassiou, P. D. Fernandez, R. Baque, X. Dupuis, and T. Casal, "SAR imaging of tropical African forests with P-band multibaseline acquisitions: Results from the AfriSAR campaign," *2016 IEEE International Geoscience and Remote Sensing Symposium (IGARSS), Beijing, China*, pp. 7521–7523, 7 2016.

[20] X. Liu, L. Zhang, X. Yang, M. Liao, and W. Li, "Retrieval of tropical forest height and above-ground biomass using airborne P- and L-band SAR tomography," *IEEE Geoscience and Remote Sensing Letters*, vol. 19, pp. 1–5, 2022.

[21] M. Pardini, J. Armston, W. Qi, S. K. Lee, M. Tello, V. Cazcarra-Bes, C. Choi, K. P. Papathanassiou, R. O. Dubayah, and L. E. Fatoyinbo, "Early lessons on combining lidar and multi-baseline SAR measurements for forest structure characterization," pp. 803–837, 7 2019.

[22] S. Tebaldini, M. d'Alessandro, L. M. H. Ulander, P. Bennet, A. Gustavsson, A. Coccia, K. Macedo, M. Disney, P. Wilkes, H.-J. Spors, N. Schumacher, J. Hanuš, J. Novotný, B. Brede, H. Bartholomeus, A. Lau, J. van der Zee, M. Herold, D. Schuettemeyer, and K. Scipal, "TomoSense: A unique 3D dataset over temperate forest combining multi-frequency mono- and bi-static tomographic SAR with terrestrial, UAV and airborne lidar, and in-situ forest census," *Remote Sensing of Environment*, vol. 290, p. 113532, 5 2023.

[23] X. Yang, S. Tebaldini, M. M. d'Alessandro, and M. Liao, "Tropical forest height retrieval based on P-band multibaseline SAR data," *IEEE Geoscience and Remote Sensing Letters*, vol. 17, pp. 451–455, 3 2020.

[24] Y. Yu, M. M. d'Alessandro, S. Tebaldini, and M. Liao, "Signal processing options for high resolution SAR tomography of natural scenarios," *Remote Sensing*, vol. 12, p. 1638, 5 2020.

[25] S. Tebaldini, F. Rocca, M. M. d'Alessandro, and L. Ferro-Famil, "Phase calibration of airborne tomographic SAR data via phase center double localization," *IEEE Transactions on Geoscience and Remote Sensing*, vol. 54, pp. 1775–1792, 3 2016.

[26] M. M. D'Alessandro and S. Tebaldini, "Digital terrain model retrieval in tropical forests through P-band SAR tomography," *IEEE Transactions on Geoscience and Remote Sensing*, vol. 57, pp. 6774–6781, 9 2019.

[27] S. Tebaldini and A. M. Guarnieri, "On the role of phase stability in SAR multibaseline applications," *IEEE Transactions on Geoscience and Remote Sensing*, vol. 48, pp. 2953–2966, 7 2010.

[28] O. Brovkina, B. Navrátilová, J. Novotný, J. Albert, L. Slezák, and E. Cienciala, "Influences of vegetation, model, and data parameters on forest aboveground biomass assessment using an area-based approach," *Ecological Informatics*, vol. 70, p. 101754, 9 2022.

[29] J. C. White, M. A. Wulder, A. Varhola, M. Vastaranta, N. C. Coops, B. D. Cook, D. Pitt, and M. Woods, "A best practices guide for generating forest inventory attributes from airborne laser scanning data using an area-based approach," *The Forestry Chronicle*, vol. 89, no. 06, pp. 722–723, 2013.

[30] P. Tompalski, J. C. White, N. C. Coops, and M. A. Wulder, "Demonstrating the transferability of forest inventory attribute models derived using airborne laser scanning data," *Remote Sensing of Environment*, vol. 227, pp. 110–124, 6 2019.

[31] J. Vauhkonen, M. Maltamo, R. E. McRoberts, and E. Næsset, *Forestry applications of airborne laser scanning*. Springer Netherlands, 2014, ch. Introduction to Forestry Applications of Airborne Laser Scanning, pp. 1–16.

[32] E. Næsset, "Predicting forest stand characteristics with airborne scanning laser using a practical two-stage procedure and field data," *Remote Sensing of Environment*, vol. 80, pp. 88–99, 4 2002.

[33] M. Vastaranta, M. A. Wulder, J. C. White, A. Pekkarinen, S. Tuominen, C. Ginzler, V. Kankare, M. Holopainen, J. Hyyppä, and H. Hyyppä, "Airborne laser scanning and digital stereo imagery measures of forest structure: comparative results and implications to forest mapping and inventory update," *Canadian Journal of Remote Sensing*, vol. 39, pp. 382–395, 11 2013.

[34] M. Neumann, S. S. Saatchi, L. M. H. Ulander, and J. E. S. Fransson, "Assessing performance of L- and P-band polarimetric interferometric SAR data in estimating boreal forest above-ground biomass," *IEEE Transactions on Geoscience and Remote Sensing*, vol. 50, pp. 714–726, 2012.

[35] M. Kuhn and K. Johnson, *Applied Predictive Modeling*. Springer New York, 2013.

[36] S. Chatterjee and J. S. Simonoff, *Handbook of Regression Analysis*. Wiley, 12 2012.

[37] L. M. H. Ulander, "Radiometric slope correction of synthetic-aperture radar images," *IEEE Transactions on Geoscience and Remote Sensing*, vol. 34, pp. 1115–1122, 1996.

[38] G. Sandberg, L. M. H. Ulander, J. E. S. Fransson, J. Holmgren, and T. Le Toan, "L- and P-band backscatter intensity for biomass retrieval in hemiboreal forest," *Remote Sensing of Environment*, vol. 115, pp. 2874–2886, 11 2011.

[39] M. Tello, V. Cazcarra-Bes, M. Pardini, and K. Papathanassiou, "Forest structure characterization from SAR tomography at L-band," *IEEE Journal of Selected Topics in Applied Earth Observations and Remote Sensing*, vol. 11, pp. 3402–3414, 10 2018.

[40] M. Schlund and M. Davidson, "Aboveground forest biomass estimation combining L- and P-band SAR acquisitions," *Remote Sensing*, vol. 10, p. 1151, 7 2018.

[41] P. J. Bennet, A. R. Monteith, and L. M. H. Ulander, "Diurnal cycles of L-band tomographic SAR backscatter in a boreal forest during summer: Observations by the BorealScat tower radar," *2023 IEEE International Geoscience and Remote Sensing Symposium (IGARSS), Pasadena, CA, USA*, pp. 2195–2198, 7 2023.

[42] A. R. Monteith and L. M. H. Ulander, "Temporal characteristics of P-band tomographic radar backscatter of a boreal forest," *IEEE Journal of Selected Topics in Applied Earth Observations and Remote Sensing*, vol. 14, pp. 1967–1984, 2021.

[43] G. B. Bonan, "Forests and climate change: Forcings, feedbacks, and the climate benefits of forests," *Science*, vol. 320, pp. 1444–1449, 6 2008.

[44] P. C. Dubois-Fernandez, T. Le Toan, S. Daniel, H. Oriot, J. Chave, L. Blanc, L. Villard, M. W. J. Davidson, and M. Petit, "The TropiSAR airborne campaign in French Guiana: Objectives, description, and observed temporal behavior of the backscatter signal," *IEEE Transactions on Geoscience and Remote Sensing*, vol. 50, pp. 3228–3241, 8 2012.

[45] T. Fatoyinbo, J. Armston, M. Simard, S. Saatchi, M. Denbina, M. Lavalle, M. Hofton, H. Tang, S. Marselis, N. Pinto, S. Hancock, B. Hawkins, L. Duncanson, B. Blair, C. Hansen, Y. Lou, R. Dubayah, S. Hensley, C. Silva, J. R. Poulsen, N. Labrière, N. Barbier, K. Jeffery, D. Kenfack, M. Herve, P. Bissiengou, A. Alonso, G. Moussavou, L. T. J. White, S. Lewis, and K. Hibbard, "The NASA AfriSAR campaign: Airborne SAR and lidar measurements of tropical forest structure and biomass in support of current and future space missions," *Remote Sensing of Environment*, vol. 264, p. 112533, 10 2021.

[46] L. M. H. Ulander, A. Gustavsson, P. Dubois-Fernandez, X. Dupuis, J. E. S. Fransson, J. Holmgren, J. Wallerman, L. Eriksson, G. Sandberg, and M. Soja, "BIOSAR 2010 - A SAR campaign in support to the BIOMASS mission," *2011 IEEE International Geoscience and Remote Sensing Symposium (IGARSS), Vancouver, BC, Canada*, pp. 1528–1531, 7 2011.

[47] M. J. Soja, G. Sandberg, and L. M. H. Ulander, "Regression-based retrieval of boreal forest biomass in sloping terrain using P-band SAR backscatter intensity data," *IEEE Transactions on Geoscience and Remote Sensing*, vol. 51, pp. 2646–2665, 5 2013.

[48] I. Hajnsek, R. Scheiber, S. Lee, L. Ulander, A. Gustavsson, S. Tebaldini, and A. Monte Guarnieri, "BIOSAR 2007: Technical assistance for the

development of airborne SAR and geophysical measurements during the BioSAR 2007 experiment," ESA-ESTEC, Tech. Rep., February 2008.

[49] I. Hajnsek, R. Scheiber, M. Keller, R. Horn, S. Lee, L. Ulander, A. Gustavsson, G. Sandberg, T. Le Toan, S. Tebaldini, A. Monte Guarnieri, and F. Rocca, "BIOSAR 2008: Final report," ESA-ESTEC, Tech. Rep., November 2009.

[50] M. J. Soja, F. Banda, P. Mazzuchelli, M. M. d'Alessandro, S. Quegan, N. Miranda, and K. Scipal, "Design and parameter estimation robustness of the global above-ground biomass estimation algorithm for ESA's 7th Earth explorer mission BIOMASS," *2023 IEEE International Geoscience and Remote Sensing Symposium (IGARSS), Pasadena, CA, USA*, 7 2023.

[51] C. A. Silva, L. Duncanson, S. Hancock, A. Neuenschwander, N. Thomas, M. Hofton, L. Fatoyinbo, M. Simard, C. Z. Marshak, J. Armston, S. Lutchke, and R. Dubayah, "Fusing simulated GEDI, ICESat-2 and NISAR data for regional aboveground biomass mapping," *Remote Sensing of Environment*, vol. 253, p. 112234, 2021.

Patrik J. Bennet is a Ph.D. student in Radio and Space Science at Chalmers University of Technology in Gothenburg, Sweden. His research focuses on radar remote sensing of forests, with emphasis on radar tomography for biomass estimation and the temporal characteristics related to forest water dynamics and vitality. He obtained his B.Sc. in Electrical Engineering and M.Sc. in Communication Engineering from Chalmers before beginning his Ph.D. studies in May 2021.

Lars M. H. Ulander (Fellow, IEEE) received the M.Sc. degree in engineering physics and the Ph.D. degree in electrical and computer engineering from the Chalmers University of Technology, Gothenburg, Sweden, in 1985 and 1991, respectively. Since 1995, he has been with the Swedish Defence Research Agency (FOI), where he is the Director of Research in Radar Signal Processing and leads the research on very high-/ultrahigh-frequency band radar. Since 2014, he has been a Professor in radar remote sensing with the Chalmers University of Technology. He is the author or coauthor of over 300 professional publications, of which more than 60 are published in peer-reviewed scientific journals. He is the holder of five patents. His research interests include synthetic aperture radar, electromagnetic scattering models, and remote sensing applications.

PLACE PHOTO HERE

Mauro Mariotti D'Alessandro Biography text here.

PLACE PHOTO HERE

Stefano Tebaldini Biography text here.